Sources of dissolved iron to oxygen minimum zone waters on the Senegalese continental margin in the tropical North Atlantic Ocean: Insights from iron isotopes

JK Klar[1,2,*], C Schlosser[3], JA Milton[1], EMS Woodward[4], F Lacan[2], IJ Parkinson[5], EP Achterberg[1,3], RH James[1]

(1) Ocean and Earth Science, National Oceanography Centre, University of Southampton, European Way, Southampton SO14 3ZH, UK

(2) LEGOS, Université de Toulouse, CNES, CNRS, IRD, UPS, 14 Avenue Edouard Belin, 31400 Toulouse, France

(3) GEOMAR Helmholtz Centre for Ocean Research, Wischhofstraße 1-3, 24148 Kiel, Germany

(4) Plymouth Marine Laboratory, Prospect Place, The Hoe, Plymouth PL1 3DH, UK

(5) School of Earth Sciences, University of Bristol, Queens Road, Bristol, BS8 1RJ, UK

*corresponding author, email address: Jessica.klar@legos.obs-mip.fr

Keywords: tropical Atlantic Ocean; iron isotopes; oxygen minimum zone; benthic iron; remineralisation; dissolved aluminium; dust; GEOTRACES

Abstract

Oxygen minimum zones (OMZs) cover extensive areas of eastern boundary ocean regions and play an important role in the cycling of the essential micronutrient iron (Fe). The isotopic composition of dissolved Fe (dFe) in shelf and slope waters on the Senegalese margin was determined to investigate the processes leading to enhanced dFe concentrations (up to 2 nM) in this tropical North Atlantic OMZ. On the shelf, the δ^{56}Fe value of dFe (relative to the reference material IRMM-014) was as low as -0.33 ‰, which can be attributed to input of dFe from both reductive and nonreductive dissolution of sediments. Benthic inputs of dFe are subsequently upwelled to surface waters and recycled in the water column by biological uptake and remineralisation processes. Remineralised dFe is characterised by relatively high δ^{56}Fe values (up to +0.41 ‰), and the contribution of remineralised Fe to the total dFe pool increases with distance from the shelf. Remineralisation plays an important role in the redistribution of dFe that is mainly supplied by benthic and atmospheric inputs, although dust inputs, estimated from dissolved aluminium concentrations, were low at the time of our study (2 to 9 nmol dFe m^{-2} d^{-1}). As OMZs are expected to expand as climate warms, our data provide important insights into Fe sources and Fe cycling in the tropical North Atlantic Ocean.

1. Introduction

Iron (Fe) is an essential element for marine phytoplankton (Martin and Fitzwater, 1988; Martin, 1990), including nitrogen fixing diazotrophs (e.g., Falkowski, 1997; Berman-Frank et al., 2001). Iron supply therefore influences the nitrogen cycle (Schlosser et al., 2014) and the strength of the biological carbon pump (Coale et al., 2004). Marine photosynthesis is responsible for about half of the global atmospheric CO_2 uptake (Le Quéré et al., 2013), and diazotroph and phytoplankton growth are limited by Fe availability in, respectively, 35 to 50 % of the world's ocean (Moore et al., 2002). Proper constraints on the sources of Fe to the oceans, and the processes that regulate its distribution, are essential for global models that are used to calculate past and future climate scenarios (e.g., Boyd and Ellwood, 2010).

The supply of Fe to the oceans is temporally and spatially variable. The low solubility of Fe in oxygenated seawater (pH ~8.1) (Liu and Millero, 2002), its highly particle reactive nature (Goldberg, 1954), and its uptake by marine microorganisms (Coale et al., 2004) lead to rapid removal of Fe from the surface ocean. Therefore, Fe concentrations tend to be highest close to source regions. Iron is mainly delivered to the ocean from atmospheric dust deposition, margin sediments, rivers, groundwater discharge and hydrothermal vents (Boyd and Ellwood, 2010, and references therein).

In the open ocean dissolved Fe (dFe; i.e. filterable through 0.4 or 0.2 μm) concentrations typically range between <0.2 to ~1 nmol L^{-1} (e.g., Klunder et al., 2011; Klunder et al., 2012; Rijkenberg et al., 2014; Resing et al., 2015; Nishioka and Obata, 2017) and are generally lowest in the surface ocean. However, dFe concentrations of 1 to 1.7 nmol L^{-1} have been observed within oxygen minimum zones (OMZs) away from coastal seas (Ussher et al., 2010; Rijkenberg et al., 2012; Fitzsimmons et al., 2013; Ussher et al., 2013; Conway and John, 2014; John et al., 2017; Milne et al., 2017). The development of OMZs occurs in "shadow zones" of eastern boundary regions where the wind-driven supply of recently ventilated water is slowed, and oxygen consumption is accentuated due to elevated biological production in surface waters caused by upwelling of nutrient rich waters and degradation of sinking organic matter (Karstensen et al., 2008). OMZs usually extend between ~100 and ~700 m water depth in regions with sluggish circulation, such as the eastern tropical Atlantic and eastern tropical Pacific (Stramma et al., 2005). Elevated dFe concentrations encountered in OMZs are attributed to remineralisation of biogenic Fe that sinks from the surface (Rijkenberg et al., 2012; Fitzsimmons et al., 2013), and transport of high dFe – low oxygen waters from the adjacent continental shelf forms another source (Ussher et al., 2010; Conway and John, 2014; Chever et al., 2015). In addition, elevated dFe concentrations off the Peru margin of the eastern tropical South Pacific have been attributed to reversible scavenging of dFe from

sinking particles (John et al., 2017). The relative importance of each of these processes for Fe supply to oxygen deficient waters is, however, poorly constrained. As anthropogenic climate change results in the expansion and intensification of OMZs in the worlds' oceans (Stramma et al., 2008b; Brandt et al., 2010; Schmidtko et al., 2017) and is postulated to have important effects on the biogeochemical cycling of many redox-sensitive elements, including Fe, as well as ecosystem functioning (Chan et al., 2008; Keeling et al., 2010), the Fe sources to OMZs need to be constrained.

The isotopic composition of dFe is a relatively new tool that can help to identify Fe supply and removal mechanisms in the ocean as well as biogeochemical processing of Fe within the ocean (e.g., Lacan et al., 2008), that cannot be provided by concentration data only. Iron isotope ratios are expressed in delta notation relative to the international reference material IRMM-014 throughout this manuscript (equation 1).

$$\delta^{56}Fe\ (‰) = \left[\frac{\left(^{56}Fe/^{54}Fe\right)_{sample}}{\left(^{56}Fe/^{54}Fe\right)_{IRMM-014}} - 1\right] \cdot 1000 \quad (1)$$

The isotopic signatures of dFe for different sources are distinct. The continental crust has an average δ^{56}Fe value of +0.09 ± 0.10 ‰ (2 SD, *n = 46*; Beard et al. (2003). The δ^{56}Fe value of atmospheric dust in the North Atlantic (~+0.07 ± 0.11 ‰; Waeles et al., 2007; Mead et al., 2013) is similar to the crustal value, but has been suggested to be modified during deposition and dissolution in surface seawater, leading to a δ^{56}Fe signature of between +0.3 and +0.7 ‰ (Conway and John, 2014), although these heavy signatures may include the influence of other processes, such as biological uptake. Fe reduction in anoxic sediments and the efflux of pore waters supply isotopically light Fe to the overlying water column, leading to typical δ^{56}Fe values in oxygenated bottom waters of between -1.25 and -0.1 ‰ (Conway and John, 2014; Chever et al., 2015; Klar et al., 2017a), and as low as -3.5 ‰ in anoxic bottom waters (John et al., 2012). In contrast, non-reductive dissolution of lithogenic material on continental margins and in the water column is thought to lead to a δ^{56}Fe of dFe between -0.3 and +0.5 ‰ (Radic et al., 2011; Homoky et al., 2013; Conway and John, 2014; Abadie et al., 2017), and an isotopic difference between dissolved and particulate Fe ($\Delta^{56}Fe_{dFe\text{-}pFe}$) of +0.27 ± 0.25 ‰ (Labatut et al., 2014). The reported isotopic signal of dFe in rivers draining into tropical oceans is -0.27 to +0.31 ‰ (Bergquist and Boyle, 2006), although the range for all of the world's rivers is larger (-1.2 to +0.8 ‰; Escoube et al., 2009; Escoube et al., 2015). The δ^{56}Fe values of all of these sources can nevertheless be modified by chemical and physical transformations within the ocean.

The main processes leading to modifications of dFe concentrations and their isotopic composition are redox reactions, organic complexation, biological uptake, remineralisation of organic matter and adsorption/desorption onto/from suspended particles. Upon delivery of dFe to the ocean from reducing sediments, rivers or hydrothermal vents, the change in ambient temperature, salinity, oxygen concentrations, pH and redox potential may lead to precipitation of Fe as, for example, Fe-(oxy)hydroxides and Fe-sulphides. Fe(II) that remains in solution after partial oxidation to Fe(III) followed by Fe(III)-(oxy)hydroxide precipitation could theoretically be up to 3.9 ‰ lighter than the initial Fe(II) pool (e.g., Bullen et al., 2001; Klar et al., 2017b). The formation of iron sulphide (FeS) minerals leads to an isotopic fractionation of $\Delta^{56}Fe_{Fe(II)\text{-}FeS} < +0.77$ ‰ (Rouxel et al., 2008). It is now clear that dFe is rapidly complexed upon delivery to the ocean, with >99 % of dFe bound to organic ligands (Gledhill and Buck, 2012) and references therein). It has been observed that organically complexed Fe has $\delta^{56}Fe$ values up to 0.6 ‰ higher than inorganic dFe (Dideriksen et al., 2008; Morgan et al., 2010). However, this value might be ligand specific and variable. Recently reported data from the Peru margin OMZ is best modelled if the expression of isotopically light dFe that remains in solution after partial oxidation of Fe(II) is muted due to formation of Fe(III)-ligand complexes (Chever et al., 2015). In the presence of sufficient light and macronutrients, Fe is rapidly taken up during primary production in the surface ocean. Opposing directions of Fe isotopic fractionation associated with biological uptake have been reported. The uptake of isotopically light Fe with an isotopic difference between the particulate and dissolved $\delta^{56}Fe$ values, $\Delta^{56}Fe_{pFe\text{-}dFe} < -0.54$ ‰ has been observed in the waters east of New Zealand and in the equatorial Pacific Ocean (Radic et al., 2011; Ellwood et al., 2015). In contrast, relatively low $\delta^{56}Fe$ values of dFe (-0.01 ‰) were observed in the deep fluorescence maximum and dFe minimum in the North Atlantic Ocean (Conway and John, 2014). Thus, it appears that the sinking of dead phytoplankton cells and their remineralisation at depth may lead to the release of both isotopically light (Ellwood et al., 2015; Radic et al., 2011) or heavy (Conway and John, 2014) Fe to the dissolved pool. Iron is highly particle reactive (Goldberg, 1954), and it is thought that adsorption/desorption of Fe onto/from particle surfaces is continuously occurring throughout the water column (Milne et al., 2017). The effects of scavenging/desorption on the isotopic composition of dFe are however not yet clear. While one study found that scavenging resulted in the preferential uptake of heavy Fe onto particles ($\Delta^{56}Fe_{dFe\text{-}scavFe} = -0.67$ ‰; Ellwood et al., 2015), results from another study indicated differences in $\delta^{56}Fe$ values of scavenged Fe relative to dFe were only small ($\Delta^{56}Fe_{dFe\text{-}scavFe} = +0.3 \pm 0.3$ ‰; Radic et al., 2011).

To constrain the processes that regulate the behaviour of Fe within OMZs, we have determined the isotopic signature of dFe from four water column profiles in the West African shelf and slope region of

the tropical North Atlantic Ocean. We use our data to identify the sources of dFe in the OMZ and assess the effects of internal processes, such as Fe-ligand formation, biological uptake, remineralisation and scavenging, as well as water mass transport and mixing, on the distribution of Fe. This work contributes to the international GEOTRACES program (www.geotraces.org).

2. Materials and methods

2.1 Cleaning procedures

Seawater samples were collected in one litre high density polyethylene (HDPE) bottles (Nalgene), which were acid cleaned following a three-step procedure. Firstly, the bottles were filled and submerged for at least 3 days in 2 % Decon. After a thorough rinse in reverse osmosis water, the bottles were filled and submerged in a 6 M hydrochloric acid (HCl, analytical grade, Fisher Scientific) bath for one week. The bottles were then rinsed with purified deionised water (Milli-Q, Merck Millipore; resistivity = 18.2 MΩ cm) and transferred into a 7 M nitric acid (HNO_3, analytical grade, Fisher Scientific) bath for another week. Finally, the bottles were thoroughly rinsed with purified deionised water, double bagged and stored in boxes until used for sampling on the ship.

Laboratory equipment used for sample processing was mainly polytetrafluoroethylene (PTFE), fluorinated ethylene propylene (FEP) or perfluoroalkoxy (PFA), with some low density polyethylene (LDPE) and polyethylene (PE) components, all cleaned thoroughly in dilute HCl and HNO_3 before and between uses.

2.2 Sample collection

Samples were collected during RRS *Discovery* cruise D361 (GEOTRACES section GA06) between the 7th February and the 19th March 2011. Water was collected from four stations, ranging from 51 to 2656 m water depth (Figure 1), using a trace metal clean conductivity-temperature-pressure (CTD) rosette system. The trace metal clean CTD (TM-CTD) rosette was equipped with 24 × 10 L OTE (Ocean Test Equipment, Inc.) bottles (with external springs, modified for trace metal work) that were mounted onto a titanium frame. The TM-CTD was deployed on a non-conducting Kevlar wire fitted with a Seabird auto-fire module that triggered the OTE bottles at pre-programmed depths. Sampling depths were selected according to salinity, temperature, dissolved oxygen concentration and transmission profiles, obtained immediately beforehand by a standard stainless steel CTD deployment. Immediately after recovery of the TM-CTD rosette, the OTE bottles were transferred into a trace metal clean container for sub-sampling.

For water filtration, OTE bottles were pressurised with oxygen-free N_2 gas at a low overpressure of 10-50 kPa. Water samples were filtered through 0.2 µm Acropak 500 filter capsules (Pall Corp.), that were pre-rinsed with ~5 L surface seawater from the trace metal clean "tow-fish", or through acid cleaned 0.45 µm polyethersulfone membrane filters (Supor, Pall Gelman). The filters were rinsed with several hundred mL of sample, followed by three rinses of the HDPE sample bottle before filling up. For Fe isotopes, three 1 L bottles were filled for each sample.

Surface seawater samples were collected with the trace metal clean "tow-fish", deployed on the side of the ship. Seawater was pumped into the clean laboratory using a trace metal clean Teflon diaphragm pump through acid washed braided PVC tubing during the ships transit (10 knots). Samples were filtered in-line through a 0.8/0.2 µm cartridge filter (AcroPak1000) into acid-washed low-density polyethylene bottles for dFe and dAl analysis.

Samples were acidified to pH ~2 with concentrated HCl (Romil, Ultra Purity Acid, UpA). Isotope samples were double bagged and stored for shipping back to the National Oceanography Centre (NOC) in Southampton for analysis. Dissolved Al samples were allowed to equilibrate for at least 24 h prior analysis on board.

2.3 Analysis of dissolved Fe concentrations and isotopes

Dissolved Fe concentrations were analysed on board using chemiluminescence flow-injection-analysis following a method outlined by (Klunder et al., 2011) and are published in Schlosser et al. (2014) and Milne et al. (2017). Iron for isotope analysis was preconcentrated using a nitriloacetic acid (NTA) Superflow resin (Qiagen) and purified by anion exchange chromatography (BioRad AG1-x8 resin; ~0.5 ml loaded onto a homemade polyethylene column). Two preconcentration protocols were used, a batch method (~0.65 ml wet resin added directly to the seawater sample), modified from (John and Adkins, 2010) and a column method (~1 ml wet resin in homemade FEP columns), based on (Lacan et al., 2010). At least 24 h before preconcentration, already acidified (pH < 2) seawater samples were adjusted to a pH of between 1.75 and 1.80. To oxidize any remaining Fe(II) to Fe(III) in the sample, H_2O_2 (Romil, UpA, Ultra Purity Reagent) was added to the samples to give a final concentration of 10 µM, 30 minutes before preconcentration. The average yield from both methods was 95 ± 8 % Fe (*n = 15*) and the procedure blank was 1.7 ± 0.5 ng Fe (*n = 11*) for the batch method and 2.3 ± 0.7 ng Fe (*n = 10*) for the column method. Sample volumes ranged from 1 to 3 L, leading to a final sample size of 100 to 350 ng Fe. When dFe concentrations were < 1.5 nmol L^{-1}, individual 1 L bottles were combined in 4 L LDPE cubitainers to increase the sample volume.

Isotopic measurements of samples were carried out in duplicate on a multi-collector inductively coupled plasma mass spectrometer (MC-ICP-MS) (Thermo Fisher Neptune) at the University of Southampton. The sample was introduced to the plasma via a desolvating inlet system, either a CETAC Aridus II or an ESI Apex-Q without a membrane to increase sensitivity (Dauphas et al., 2009), using a 75 µL min^{-1} Teflon nebuliser. The MC-ICP-MS was fitted with an x-type skimmer cone to increase ion transmission and was run in high-resolution mode using a narrow slit (25 µm). In addition to the four Fe isotopes (^{54}Fe, ^{56}Fe, ^{57}Fe, ^{58}Fe), ^{53}Cr and ^{60}Ni were also measured, to correct any isobaric interference of ^{54}Cr on ^{54}Fe and ^{58}Ni on ^{58}Fe, assuming that the instrumental mass bias is the same for Fe, Cr and Ni and that $^{54}Cr/^{53}Cr$ and $^{58}Ni/^{60}Ni$ ratios are equal to the natural average (Dauphas et al., 2009). Instrumental mass bias was corrected by addition of a double spike (0.49 % ^{54}Fe, 0.71 % ^{56}Fe, 45.73 % ^{57}Fe and 53.08 % ^{58}Fe) prior to sample processing at a ~1:1 sample to spike ratio. The typical ^{56}Fe ion beam size was between 0.04 and 0.10 V ppm^{-1}. Measured $^{56}Fe/^{54}Fe$ ratios of the sample- or standard-spike mixture were instrumental blank subtracted (< 0.06 %) and the sample or standard $^{56}Fe/^{54}Fe$ ratios were obtained by iterative deconvolution, while at the same time correcting for instrumental mass bias and Cr and Ni interferences (Albarède and Beard, 2004). $^{56}Fe/^{54}Fe$ sample ratios are expressed as $\delta^{56}Fe$ relative to the average $^{56}Fe/^{54}Fe$ value for the Fe isotope reference material IRMM-014 (Institute for Reference Materials and Measurements) determined during the same analytical session (equation 1). The external precision and accuracy of the isotope measurements was assessed by multiple analyses of an Fe isotope standard during each analytical session. The average value of ETH (Eidgenössische Technische Hochschule, Zürich) hematite standard for all analytical sessions was +0.52 ± 0.07 ‰ (2 SD, *n = 54*). This value compares well with previous measurements of the ETH hematite standard reported in (Lacan et al., 2010) (+0.52 ± 0.08 ‰, 2 SD, *n = 81*). Analytical replicates, which consisted of splitting the sample and replicating the entire analytical procedure, of samples 6_16 and 8_13 (Table 1), resulted in differences between replicates that are within the external reproducibility of the ETH standard.

We have further validated our Fe isotope method by blind analysis of two seawater samples that had already been analysed in F. Lacan's lab (LEGOS, Toulouse, France). The seawater samples were collected from Station 14 during Cruise *R/V Kilo Moana 0625* in 2006 and Fe isotope results obtained at LEGOS are published in Radic et al. (2011). Fe concentrations were sub nano-molar, which is characteristic of open ocean seawater. By preconcentrating a similar quantity of Fe to the samples in this study, we obtained $\delta^{56}Fe$ values of +0.07 ± 0.07 ‰ (*n = 2*) for sample 14-2 at 849 m depth (*vs.* +0.22 ± 0.05 ‰ in Radic et al., 2011) and +0.34 ± 0.06 ‰ (*n = 2*) for sample 14-6 at 198 m depth (*vs*. +0.40 ± 0.06 ‰ in Radic et al.,

2011). These replicate analyses are within the range of inter-lab reproducibility (± 0.17 ‰) for 0.4 nmol L^{-1} dFe, reported in Boyle et al. (2012) and Conway et al. (2016).

2.4 Analysis of dissolved aluminium concentrations

Dissolved aluminium (dAl) concentrations were determined on board by flow injection analysis using a lumogallion-Al fluorescence technique originally developed by Resing and Measures (1994) and modified according to Brown and Bruland (2008). The analytical procedure was validated by analysing North Atlantic GEOTRACES Reference Seawater. GD-23 yielded 18.2 ± 1.0 nmol kg^{-1} dAl, *n = 4* (*vs.* a consensus value of 17.7 ± 0.2 nmol kg^{-1}) and GS-57 yielded 27.1 ± 1.1 nmol kg^{-1} dAl, *n = 5* (*vs.* a consensus value of 27.5 ± 0.2 nmol kg^{-1}).

2.5 Auxiliary data

A Sea-Bird 911 plus CTD sensor, fin-mounted secondary temperature and conductivity sensors, a Digiquartz pressure sensor, a fluorometer sensor and a transmissiometer sensor were mounted on the titanium rosette frame. Sensors were cross-calibrated with discrete seawater analyses using the Winkler method for oxygen (Carpenter, 1965) and conductivity measurements of a certified reference material for salinity. Chlorophyll-a content was monitored using a fluorometer fitted on the rosette frame and the manufacturer's calibration was applied. More details on sensors and calibration methods employed during D361 can be found at the British Oceanographic Data Centre (www.bodc.ac.uk).

Concentrations of seawater nitrate, nitrite, silicate, ammonium and phosphate were determined on board the RRS *Discovery*, using a 5-channel segmented flow auto-analyser (Bran and Luebbe AAIII) (Woodward and Rees, 2001).

3. Results

3.1 Hydrography and oxygen content

Off the coast of Senegal, four main water masses were identified from potential temperature, salinity and potential density signatures (Figure 2). The surface 40 m consisted of Tropical Surface Water (TSW; σ_θ < 25.8 kg m^{-3}) (Stramma et al., 2005; Stramma et al., 2008a). Between the isopycnals (σ_θ) 25.8 and 27.1 kg m^{-3}, at temperatures above 8 °C, subsurface waters down to 500 m depth mainly consisted of South Atlantic Central Water (SACW) (Stramma et al., 2005), which is formed from Indian Ocean Central Water, and transferred to the Atlantic Ocean by the Aghulas and Benguela currents (Stramma and England, 1999). After flowing northwards with the Benguela Current, SACW flows westward into the

tropical Atlantic with the South Equatorial Current (SEC) (Stramma and Schott, 1999). Below 500 m water depth, northward flowing Antarctic Intermediate Water (AAIW) was identified by a pronounced salinity minimum at ~34.8 PSU, elevated oxygen and nutrient concentrations, and was observed at stations 2 and 3, with its core at 900 m depth (Stramma et al., 2005). Southward flowing North Atlantic Deep Water (NADW) was observed below 1200 m depth to the seafloor at Station 2 (σ_θ > 27.6 kg m^{-3}), and was characterised by its relatively high salinity (Stramma and England, 1999).

The flow field in the upper 800 m of the northeastern subtropical Atlantic is controlled by a wind driven subtropical gyre (Stramma et al., 2005) (Figure 1). Upwelling occurs near the coast of Senegal and Mauritania, as well as in the Guinea Dome (Schott et al., 2004). Coastal upwelling replaces the water moved offshore by Ekman transport, driven by equatorward winds (Stramma et al., 2005). Upwelling in the Guinea Dome is due to cyclonic circulation, associated with the North Equatorial Counter Current (NECC), the northern NECC (nNECC) and the North Equatorial Undercurrent (NEUC) (Stramma et al., 2005; Stramma et al., 2008a) (Figure 1). The Guinea Dome and its related circulation are weakened during the winter, even though they exist throughout the year (Siedler et al., 1987).

In the upper 40 m of the water column, oxygen concentrations were > 200 µmol kg^{-1}. Oxygen concentrations were < 70 µmol kg^{-1} at depths between ~40 and ~900 m (the approximate extension of these waters at 400 m depth is shown in Figure 1). Oxygen depleted waters roughly coincided with the extension of SACW and the upper part of AAIW (Figure 2). Oxygen concentrations reached a minimum of ~ 45 µmol kg^{-1} at around 400 m depth at Stations 2 and 3. NADW was well oxygenated, and oxygen concentrations were > 200 µmol kg^{-1} near the seafloor. Our observations agree with previous reports of oxygen concentrations > 35 µmol kg^{-1} for the OMZ in the tropical North Atlantic Ocean, compared to concentrations within the OMZ of the eastern tropical Pacific Ocean of < 2 µmol kg^{-1} (Stramma et al., 2008b). The OMZ in the tropical North Atlantic Ocean consists of poorly ventilated upwelled waters, flowing westward from the African coast. The OMZ is contained by ventilation from below by AAIW; in the north and south by the eastward flowing zonal jets; and in the west by subtropical gyre waters (Stramma et al., 2005).

3.2 Distributions of dFe, δ^{56}Fe and macronutrients

Dissolved Fe concentrations in the water column ranged between 1.33 nmol L^{-1} and 6.3 nmol L^{-1} (Figure 4 and Table 1). On the shelf, the highest dFe concentrations were observed near the seafloor and lowest concentrations in the surface waters, indicating benthic supply. By contrast, the slope stations (2 and 3) showed a mid-depth maximum between 300 m and 1100 m (up to 3.77 nmol L^{-1}) and rather similar dFe

concentrations above and below (~ 1.5 nmol L^{-1}) of this feature. Dissolved Fe showed an approximately linear relationship with nitrate and phosphate (Figure 3), for which the slope of the regression line was steeper for the offshore stations 2 and 3 than for the two shelf stations 4 and 5.

δ^{56}Fe values for dFe ranged between -0.33 and +0.41 ‰ (Figure 4 and Table 1). δ^{56}Fe values were lowest over the shelf (~ -0.3 ‰) close to the seafloor, and increased towards the crustal value (+0.09 ± 0.10 ‰, 2 SD; Beard et al. (2003) higher up in the water column and away from the shelf (Figure 4 and Table 1).

On the slope, Station 3 (1041 m water depth) displayed lowest δ^{56}Fe values (between -0.27 and -0.15 ‰) in oxygen depleted waters. Higher δ^{56}Fe values were observed at 200 m (+0.06 ‰) and 600 m depth (-0.08 ‰). The highest δ^{56}Fe values (-0.06 to +0.41 ‰) were observed at the furthest offshore Station 2 (2656 m water depth). Here, δ^{56}Fe values increased from -0.06 ‰ at 200 m depth to +0.41 ‰ at 500 m depth. Between 600 m and the seafloor, there was little variation in δ^{56}Fe, with values around +0.1 ‰.

4. Discussion

4.1 Benthic supply of dFe

On the Senegalese shelf, elevated dFe concentrations (up to 6.35 nmol L^{-1}) in the water column close to the seafloor are indicative of a sedimentary Fe source to the overlying waters. This is consistent with other studies that have shown that shelf sediments are a source of dFe to the overlying water column even if the water column is oxygen replete (e.g., Mackey et al., 2002; Planquette et al., 2007; Conway and John, 2014; Marsay et al., 2014; Klar et al., 2017a). Moreover, the consideration of benthic Fe supply to seawater in biogeochemical models leads to an improved reproduction of dFe distributions (Siedlecki et al., 2012; Tagliabue et al., 2017). The release of dFe from seafloor sediments can be broadly classified into three categories: (i) dissimilatory iron reduction (DIR), (ii) non-reductive dissolution (NRD) and (iii) decomposition of organic matter recently transferred to the surface layer of sediments. The low δ^{56}Fe values (down to -0.33 ‰) associated with high dFe concentrations in bottom waters on the Senegalese shelf are indicative of a reduced Fe source. Previous studies (e.g., John et al., 2012; Chever et al., 2015; Klar et al., 2017a) have shown that low δ^{56}Fe values in bottom waters correspond to efflux of Fe(II) across the sediment-water interface; this Fe(II) is produced by DIR in reducing sediments. However, δ^{56}Fe values associated with DIR are usually lower than those observed in our study area. Hence, we explore the possible mechanisms that could lead to the observed isotopic signals.

DIR occurs under anoxic conditions by microbial reduction of Fe(III) to Fe(II) (e.g., Canfield, 1989; Burdige, 2006). Fe(II) is soluble and is released into pore waters, yielding Fe(II) concentrations in the

millimolar range, that has a light isotopic signature ($\delta^{56}Fe$ = -2 to -1 ‰; Severmann et al., 2006; Homoky et al., 2009; Henkel et al., 2016; Klar et al., 2017a). Upward diffusing Fe(II) is rapidly oxidised to Fe(III) when it encounters oxygenated pore waters or overlying oxygenated bottom water (Millero et al., 1987), with the subsequent formation of insoluble amorphous Fe-(oxy)hydroxide minerals at seawater pH (Liu and Millero, 2002; Ussher et al., 2004). As Fe(III) is removed from pore waters, the isotopic composition of Fe that remains in solution shifts towards lower values approaching the sediment-water interface (down to -3.5 ‰; Severmann et al., 2010). These field observations agree with experimental observations that have shown that the equilibrium fractionation between Fe(II) and Fe(III) results in the $\delta^{56}Fe$ value of aqueous Fe(III) being up to 3.5 ‰ higher than that of the coexisting aqueous Fe(II) (e.g., Welch et al., 2003). Hence, the $\delta^{56}Fe$ value of dFe depends on the proportion of Fe(III) removed from the dissolved phase through precipitation (e.g., Dauphas and Rouxel, 2006; Klar et al., 2017b). If DIR was the main process supplying high dFe concentrations to bottom waters on the Senegalese shelf, lower $\delta^{56}Fe$ values are expected. For example, $\delta^{56}Fe$ values of as low as -3.45 ‰ have been measured in low-oxygen (< 5 µmol kg^{-1}) bottom waters overlying reducing sediments along the Californian margin (John et al., 2012). However, at the same location, $\delta^{56}Fe$ values increased with increasing oxygen concentrations in the water column, such that at oxygen concentrations similar to those found within the OMZ in our study (~ 50 to 75 µmol kg^{-1}), dFe ranged from 2.4 to 4.3 nmol L^{-1} and $\delta^{56}Fe$ values ranged from -1.13 to -0.8 ‰. Our results are within the high-end spectrum of $\delta^{56}Fe$ values found in OMZ waters on the western South American margin, ranging from -1.3 to -0.3 ‰ (Chever et al., 2015; Fitzsimmons et al., 2016; John et al., 2017), and are comparable with $\delta^{56}Fe$ values found in OMZ waters on the West African margin further north (down to -0.5 ‰; Conway and John, 2014). Lowest $\delta^{56}Fe$ values (down to -1.25 ‰) were associated with the highest proportions (up to 100 %) of Fe(II) in the dissolved pool (Chever et al., 2015), which provided evidence for a benthic Fe(II) source. Similarly, Scholz et al. (2014) inferred a $\delta^{56}Fe$ value of -0.44 ‰ for dFe supplied to OMZ waters by Peru margin sediments. In addition, a light benthic iron isotope signal ($\delta^{56}Fe$ down to -1.02 ‰) was also observed in oxygen-saturated bottom waters in a temperate shelf sea (Klar et al., 2017a).

The relatively higher $\delta^{56}Fe$ values (down to -0.33 ‰) in low oxygen bottom waters (~50 – 100 µmol kg^{-1}) on shelf stations 4 and 5 (Figure 4, Table 1) may therefore reflect the presence of benthic inputs of reduced Fe that has been modified during transport across the sediment-seawater interface and/or additional inputs of Fe from other sources. Non-reductive dissolution (NRD) of lithogenic material occurs in the presence or absence of oxygen in the water column (Radic et al., 2011) and sediment porewaters (Homoky et al., 2013). It is suggested that during this process, both dissolution of particles and

adsorption of dFe onto particles occur simultaneously, with a net release of dFe from particles (Radic et al., 2011; Labatut et al., 2014; Abadie et al., 2017). Dissolved Fe with a heavier isotopic composition than particulate Fe ($\Delta^{56}Fe_{dFe\text{-}pFe}$ ~ +0.2 ‰; Radic et al., 2011; Labatut et al., 2014) has been attributed to NRD, with observed δ^{56}Fe values of +0.22 ‰ in oxic sediment pore waters (Homoky et al., 2013) and from -0.3 to +0.4 ‰ in seawater (Radic et al., 2011; Labatut et al., 2014; Abadie et al., 2017). However, along the coast of South Africa, where atmospheric deposition and the supply of lithogenic material to sediments are low, benthic Fe fluxes associated with NRD have been found significantly lower (0.11 to 0.23 µmol dFe m^{-2} d^{-1}; Homoky et al., 2013) than those associated with DIR (400 to 866 µmol dFe m^{-2} d^{-1}; (Severmann et al., 2010; Noffke et al., 2012). By contrast, relatively high dFe concentrations associated with isotopic signals characteristic of NRD have been measured in the water column in the western North Atlantic Ocean (Conway and John, 2014), where atmospheric deposition fluxes are intermediate (Jickells et al., 2005). In addition, Labatut et al. (2014) calculated large fluxes of dFe (on average 860 µmol dFe m^{-2} d^{-1}) associated with NRD of continental particles in the water column close to Papua New Guinea. Our study area lies within a high dust deposition area (Jickells et al., 2005), and therefore, NRD of rapidly accumulating "new" lithogenic material on the seafloor may make an important contribution to the total benthic Fe flux in our study area, and would explain the shift towards higher δ^{56}Fe values than expected for DIR-sourced Fe in bottom waters. Rivers (the Gambia River and the Casamance River) may also be an important source of lithogenic material to our study area. However, to date there is no data of particulate fluxes from these rivers to the adjacent shelf.

The upwelling area of the eastern (sub)tropical North Atlantic Ocean is highly productive, leading to large amounts of organic material (dead phytoplankton cells, faecal pellets, etc) continuously being exported into deeper waters and deposited on the seafloor (Broecker, 1974; Eppley and Peterson, 1979). This organic matter can be rapidly remineralised in the surface layer of the sediments (e.g., Klar et al., 2017a), leading to the release of nutrients, including dFe, to pore waters and bottom waters. Though we have no supporting data, the decomposition of organic matter at the sediment-water interface could be releasing dFe with relatively high δ^{56}Fe values to bottom waters. The release of dFe from remineralisation of organic matter and its isotopic signature will be further discussed in section 4.3.

The stabilisation of Fe in bottom waters by organic complexation could partly prevent precipitation of Fe(III)-(oxy)hydroxides, facilitating the transport of pore water Fe into overlying bottom waters (Jones et al., 2011; Hioki et al., 2014). Since relatively low benthic δ^{56}Fe signals (<-0.2 ‰) were also observed some >600 m above the seafloor in OMZ waters on the slope (Station 3; Figure 4), we suggest that a significant

proportion of the pore water dFe that is transferred to overlying waters is immediately complexed with organic ligands, allowing offshore transport. Organic ligands may be directly supplied to sediment pore waters by degradation of organic material. Complexation to organic ligands most likely favours heavy Fe isotopes, with the δ^{56}Fe of ligand bound Fe being up to 0.6 ‰ higher than that of the inorganic Fe fraction (Dideriksen et al., 2008; Morgan et al., 2010), hence, justifying a shift towards heavier isotopic compositions of the benthic Fe signal observed in bottom waters. Dissolved Fe stabilisation due to complexation with organic ligands at the sediment-water interface has also been suggested in previous studies (e.g. (Klar et al., 2017a), where Fe isotopic signals shifted from as low as -3 ‰ in anoxic pore waters to up to -0.1 ‰ in oxygen saturated bottom waters.

Hence, a combination of DIR and NRD of margin sediments, remineralisation of organic matter and complexation of dFe with organic ligands at the sediment-water interface may all influence bottom water δ^{56}Fe values (down to -0.3 ‰) on the Senegalese margin. Our iron isotope data are similar to those measured in bottom waters in the eastern tropical North Atlantic Ocean north of Cape Verde Islands, where low δ^{56}Fe values of down to -0.5 ‰ were attributed to dFe release from reducing sediments into a water column with oxygen levels >220 µmol kg^{-1} (Conway and John, 2014). In their study, however, the shallowest station close to the African shelf was ~ 3000 m deep. Our stations, located ~ 6° to the south in shallower waters therefore provide new information on δ^{56}Fe in slope and shelf waters. Benthic inputs of dFe on the Mauritanian shelf, at ~18 °N, with diffusive Fe fluxes (10 and 30 µmol m^{-2} d^{-1}) from shelf sediments (<200 m depth) to bottom waters with <50 µmol kg^{-1} oxygen, determined from pore water Fe concentrations (Lomnitz, 2017) were somewhat lower than those measured on the Californian shelf (<10 to >300 µmol m^{-2} d^{-1}) using benthic chambers (Severmann et al., 2010). Thus high benthic dFe fluxes appear to be associated with very low bottom water oxygen concentrations (i.e., <2 µmol kg^{-1} on the Californian shelf *versus* ~ 50 µmol kg^{-1} on the west African margin). However, the generally higher δ^{56}Fe values on the west African margin (~-0.3 ‰; this study; Conway and John, 2014), compared to those on the western South American margin (-1.3 to -0.3 ‰; Chever et al., 2015; Fitzsimmons et al., 2016; John et al., 2017), provide new information on the processes that regulate the benthic flux of dFe.

4.2 Atmospheric supply of Fe to the surface ocean

The study area is located in close proximity to the Sahara and Sahel deserts, which deliver large amounts of dust to the North Atlantic Ocean (Kramer et al., 2004; Jickells et al., 2005; Patey et al., 2015). Dissolved aluminium (dAl) is a nearly conservative tracer of lithogenic material in seawater (Measures and Brown,

1996), as it is only removed by scavenging processes (Moran and Moore, 1992) with minor incorporation into siliceous frustules of diatoms (Gehlen et al., 2002). Assuming that dAl in the surface mixed layer is entirely supplied by atmospheric dust, that dust is composed of 8.2 % w/w Al (Taylor, 1964), that Al solubility from Saharan dust is 13 ± 10 % (Buck et al., 2010), and that the residence time of dAl is 1.2 ± 0.5 years in tropical Atlantic waters (Dammshäuser et al., 2011), the dust flux was estimated to be 0.019 ± 0.19 g m^{-2} y^{-1} on the shelf and 0.023 – 0.080 g m^{-2} y^{-1} on the slope (Table 2). Assuming that dust is composed of 5.6 % w/w Fe (Taylor, 1964) and that Fe solubility from Saharan dust is 4 ± 2 % (Buck et al., 2010), the dust derived soluble Fe flux was between 0.002 and 0.009 µmol Fe m^{-2} d^{-1} (Table 2).

The soluble Fe fluxes from aerosols estimated from dAl concentrations were an order of magnitude lower than those determined from aerosol measurements during the same cruise (Milne et al., 2017), i.e., 0.002 ± 0.002 µmol m^{-2} d^{-1} versus 0.075 µmol m^{-2} d^{-1} on the shelf and 0.003 to 0.009 µmol m^{-2} d^{-1} versus 0.074 µmol m^{-2} d^{-1} on the slope, respectively. Slight differences between the methods are expected, as aerosol fluxes derived from dAl measurements in surface waters represent average fluxes over ~ 1.2 years, and aerosol fluxes calculated from dAl concentrations are highly dependent on Al residence time, which is, in turn, controlled by particle scavenging. More critically, however, dust fluxes are highly variable because of the episodic and complex nature of dust dynamics in the atmosphere (e.g., (Jickells et al., 2016). Our results suggest that dust-derived dFe inputs were low on the Senegalese shelf and slope regions at the time of our study, and although the soluble Fe flux from aerosols was slightly higher in the open ocean during the same cruise (0.135 µmol m^{-2} d^{-1}; Milne et al., 2017), they were also low relative to aerosol fluxes measured on the West African margin during dust storms (up to 74 µmol Fe m^{-2} d^{-1}; Croot et al., 2004). Hence, atmospheric deposition and sedimentation of lithogenic material, and potentially input of dFe from NRD, is likely to be more significant at other times of the year in our study area, and could be contributing to background dFe concentrations in the water column, which may be stabilised by complexation to organic ligands (Conway and John, 2014).

Assuming a residence time of dFe of 0.7 years in North Atlantic tropical gyre surface waters (Ussher et al., 2013), soluble Fe fluxes from dust can be converted to dust derived dFe concentrations in the surface mixed layer (Table 2). Measured dFe concentrations were consistently higher than dFe concentrations calculated from dAl derived fluxes, and lower than dFe concentrations obtained from aerosol measurements. Nevertheless, our data indicate that atmospheric dust was likely to supply > 10% of dFe to surface waters in our study area.

We have no $\delta^{56}Fe$ measurements from within the surface mixed layer (SML, 11 to 19 m thick) and dFe isotopic compositions are likely significantly modified below the SML due to scavenging and remineralisation processes. Hence, we are not able to directly assess the isotopic composition of dust-derived dFe in our study area. However, surface waters at 25 m depth on the shelf were characterised by higher $\delta^{56}Fe$ values (-0.11 to +0.03 ‰), and lower dFe concentrations (up to 3 nmol L^{-1}), compared to bottom waters (Figure 4). The shift towards higher $\delta^{56}Fe$ values between 40 m and 25 m depth is consistent with input of dust-derived dFe to the surface ocean. In support of this, NRD of sinking lithogenic material would lead to the release of dFe with $\delta^{56}Fe$ values of +0.27 ± 0.25 ‰ (Labatut et al., 2014), which is higher than that of the lithogenic material ($\delta^{56}Fe$ ~ +0.07 ± 0.11 ‰; Mead et al., 2013; Waeles et al., 2007). In addition, high $\delta^{56}Fe$ values of +0.3 to +0.7 ‰ have been measured in the SML to the north of the Cape Verde islands in the North Atlantic Ocean (Conway and John, 2014). This has been attributed to the formation of strong Fe-ligand complexes during dust dissolution, which preferentially incorporate the heavier Fe isotopes ($\Delta^{56}Fe_{LFe\text{-}dFe}$ = 0.6 ‰; Dideriksen et al., 2008; Morgan et al., 2010). Hence, NRD of sinking dust particles may explain the high $\delta^{56}Fe$ values, relative to inputs of dFe from DIR (see section 4.1), throughout the entire water column on the shelf. Since atmospheric dust inputs to our study area can be significantly more important on an episodic basis, these could produce high background $\delta^{56}Fe$ values of dFe in seawater (Conway and John, 2014). To properly assess the effects of atmospheric deposition on the isotopic composition of dFe in seawater, $\delta^{56}Fe$ analyses of aerosols and suspended particulate material offshore Senegal are required.

4.3 Fe isotopic fractionation by biological activity

Concentrations of chlorophyll-a indicated that levels of biological activity in the surface waters were high, with levels up to ~1.5 µg L^{-1} on the shelf and up to 2 µg L^{-1} on the slope (Figure 4). Maximum Chl-a and lowest transmittance were measured immediately below the surface layer (0 to 15 m depth) and thus above the depth of our shallowest Fe isotope sample. It is important to note that significant changes in $\delta^{56}Fe$ values linked to high biological activity are expected in surface waters. Uptake of isotopically light Fe linked to biological activity has previously been observed ($\Delta^{56}Fe_{pFe\text{-}dFe}$ < -0.54 ‰; (Radic et al., 2011; Ellwood et al., 2015). By contrast, (Conway and John, 2014) recorded relatively light $\delta^{56}Fe$ values of dFe (e.g., -0.01 ‰ *vs.* +0.20 ‰ above and below) associated with the deep fluorescence maximum (136 m) in the North Atlantic Ocean. John et al. (2017) observed a decrease in $\delta^{56}Fe$ of dFe in the upper few hundred metres and suggested this was due to biological uptake; however, this was not observed in all their profiles. The direction of Fe isotopic fractionation could depend on phytoplankton type.

Even though we were not able to assess the isotopic fractionation of Fe associated with biological uptake directly, we were able to do this indirectly by investigating remineralisation of sinking organic material throughout the water column. Remineralisation of sinking organic material plays an important role in recycling Fe in the ocean (e.g., Rijkenberg et al., 2012; Fitzsimmons et al., 2013). The amount of remineralised dFe in the water column below 100 m depth was calculated from estimates of apparent oxygen utilisation (AOU), assuming an AOU/C ratio of 1.6 (Martin et al., 1987) and a Fe/C ratio of 15 µmol Fe/mol C, measured in phytoplankton cells on the west African margin (Twining et al., 2015) (Figure 5). This ratio is similar to that estimated in the eastern tropical North Atlantic during cruise AMT15 (13 µmol Fe/mol C; Ussher et al. (2013). Our calculations suggest that remineralisation was a significant source of dFe, especially within the OMZ (between 40 and 900 m depth). The apparent common source of Fe and P or N, as indicated by the correlation between Fe and P or N in the water column (Figure 3), is also suggestive of significant remineralisation of sinking dead phytoplankton cells. Note that, for some samples, remineralised Fe appears to constitute > 100 % of dFe (Figure 5); this suggests that removal of dFe by particle scavenging processes was significant in the water column. Scavenging of dFe onto biogenic and non-biogenic particles and exchange of Fe between the dissolved and particulate phases are continuous processes and could overprint the isotopic signatures of benthic or atmospheric inputs and remineralisation. Since the extent of Fe isotopic fractionation associated with particle scavenging and desorption are not well known (Radic et al., 2011; Labatut et al., 2014; Ellwood et al., 2015), these processes are ignored in subsequent discussions.

Higher levels of remineralisation are associated with relatively heavy Fe isotope signatures (Figure 6). It has been shown that remineralisation of organic material is less effective in OMZs (Cavan et al., 2017), and therefore, it is not certain if the high δ^{56}Fe values reflect remineralisation of the entire biogenic Fe pool or that of an unknown fraction. Other processes such as adsorption/desorption of Fe onto/from particles and NRD of lithogenic particles could overprint δ^{56}Fe values throughout the water column, however, we assume that these changes are relatively small where remineralisation is high. At Station 3, the proportion of remineralised dFe was highest at 600 m depth (Figures 4 and 5), where the δ^{56}Fe value of dFe was -0.08 ‰. At Station 2, the proportion of dFe supplied by remineralisation was highest within the OMZ and correlated positively with δ^{56}Fe values (+0.02 to +0.41 ‰), including a highest δ^{56}Fe value of +0.41 ‰ at 500 m depth. Interestingly, the highest δ^{56}Fe values were associated with relatively low dFe concentrations at both stations, suggesting rapid scavenging onto particles. Hence, our data are consistent with biological uptake of heavy dFe isotopes in surface waters, followed by release of heavy dFe isotopes during remineralisation of this material as it sinks throughout the water column and rapid

scavenging of some part of the remineralised dFe onto sinking particles. Our results contradict previous studies, which suggested that biological Fe uptake incorporates the lighter isotopes (Ellwood et al., 2015; Radic et al., 2011), but they are consistent with the findings of Conway and John (2014), who reported that isotopically light dFe was associated with the deep fluorescence maxima and the dFe concentration minima in the North Atlantic.

4.4 Isotopic signatures within water masses

Between 700 and 1100 m water depth, AAIW was present at stations 2 and 3. The δ^{56}Fe values in this water mass were ~ +0.1 ‰ (*n = 3*) at Station 2 and -0.30 to -0.08 ‰ (*n = 4*) at Station 3. AAIW was located immediately above the seafloor at Station 3, with enhanced dFe concentrations and low δ^{56}Fe values indicating a relatively strong supply of benthic dFe to bottom waters, overwriting the isotopic signature of AAIW. In previous studies, it has been observed that AAIW transports isotopically light Fe (-0.37 to -0.17 ‰) within the southern hemisphere basins of the Atlantic and Pacific Oceans (Conway et al., 2016; Fitzsimmons et al., 2016; Abadie et al., 2017). The Fe isotopic signature of AAIW is significantly modified at the equator in the Pacific (+0.22 ‰, Radic et al., 2011) and close to Papua New Guinea (+0.06 to +0.44 ‰; Radic et al., 2011; Labatut et al., 2014). Abadie et al. (2017) observed that the light δ^{56}Fe values may originate from the dilution of Upper Circumpolar Deep Water (UCDW; ~ -0.8 ‰), as AAIW originates from the subduction of Antarctic Surface Water (AASW), which in turn results from the upwelling of UCDW. We suggest that the δ^{56}Fe values we observed in AAIW are significantly modified by remineralisation, sorption/desorption processes and benthic input of new dFe.

At Station 2 in the present study, NADW was present at depths below 1100 m, and had a δ^{56}Fe value of +0.09 to +0.12 ‰ (*n = 2*) and dFe concentrations of 1.3 to 1.7 nmol L^{-1}. Reported δ^{56}Fe values for NADW differ significantly in the literature. In the North Atlantic Ocean, Conway and John (2014) reported δ^{56}Fe values of ~ +0.21 ‰ at ~ 2000 m depth for a profile over the continental slope at ~ 18° W, and δ^{56}Fe values of ~ +0.7 ‰ at 2000 m depth at 30° W in the open ocean. Near Bermuda, the δ^{56}Fe of NADW ranged from +0.2 to +0.56 ‰ (Boyle et al., 2012; John and Adkins, 2012; Conway et al., 2013; Conway and John, 2014; Conway et al., 2016). NADW measured at ~3000 m depth in the Southern Ocean has δ^{56}Fe values of between +0.17 to +0.33 ‰ (Conway et al., 2016; Abadie et al., 2017). This suggests that the isotopic composition of NADW is slightly modified during its journey southwards. Isotopic modifications of dFe could be due to: (i) exchange between the dissolved and particulate Fe pools (Radic et al., 2011; John and Adkins, 2012; Labatut et al., 2014; Ellwood et al., 2015), and (ii) non-reductive dissolution of sinking particles (Abadie et al., 2017). Thus, due to the short residence times and reactivity

of Fe, and the supply of new Fe close to source regions, the isotopic composition of the dissolved Fe pool is continuously modified and it is clear that $\delta^{56}Fe$ cannot be applied as a conservative water mass tracer.

4.5 Origin of elevated dFe concentrations in low oxygen waters off the shelf

The elevated dFe concentrations observed in the OMZ (between 40 and 900 m depth) at Station 2 may originate from offshore advection of high dFe containing shelf waters (e.g., Conway and John, 2014), remineralisation of sinking particles (e.g., Fitzsimmons et al., 2013), and net release of dFe from particle surfaces (Milne et al., 2017). $\delta^{56}Fe$ values can be explained by mixing between high dFe concentration, low $\delta^{56}Fe$ shelf waters and low dFe concentration, high $\delta^{56}Fe$ offshore water masses (Figure 7a). On the shelf, a positive correlation between oxygen concentrations and $\delta^{56}Fe$ values could be an artefact due to larger amounts of oxygen being consumed in deeper waters combined with poor ventilation (Figure 7b). We cannot assume that isotopic signatures are solely governed by mixing processes, and hence, explore other possibilities below.

We have estimated the amount of dFe released to the water column due to remineralisation, and this was up to 2.1 nmol L^{-1} within low oxygen waters on the slope (Figures 4 and 5; section 4.3). The contribution of remineralised dFe to the total dFe concentration measured in the low oxygen waters was 56 to 170 % (average 88 ± 36 %, *n = 11*) at Station 3, and 94 to 150 % (average 118 ± 22, *n = 9*) at Station 2 (Figure 5). Hence, the importance of remineralised dFe increased with distance from the shelf. The AOU was positively correlated with dFe concentrations (R^2 = 0.4; Figure 6a), and samples with a high proportion of remineralised dFe tended to have the highest $\delta^{56}Fe$ values on the slope (Section 4.3; Figure 6b).

"Excess" dFe (dFe supplied from processes other than remineralisation) correlated with low $\delta^{56}Fe$ values on the slope (Figure 6b). For this reason, excess dFe is assumed to be principally derived from benthic Fe inputs that appeared to be advected laterally from the adjacent shelf. On the slope at Station 3, excess dFe concentrations were 0.6 ± 0.7 nmol L^{-1} (*n = 11*), constituted up to 1.6 nmol L^{-1} of total dFe at 500 and 800 m depth in low oxygen waters and were associated to relatively low $\delta^{56}Fe$ values (as low as -0.32 ‰ at 500 m depth). At Station 2, excess dFe concentrations were very low within low oxygen waters, so relatively high dFe concentrations are attributed to remineralisation.

The presence of benthic dFe in OMZ waters at slope Station 3 (Figure 4) could be facilitated by advection of shelf waters by the westward flowing NECC and the nNECC. This is supported by observations of relatively high horizontal dFe fluxes below the SML on the shelf (5185 µmol dFe m^{-2} d^{-1}) and slope (94.4

551 µmol dFe m^{-2} d^{-1} at Station 3; Figure 8; Milne et al., 2017). Benthic sources of dFe are less obvious at
552 Station 2, coincident with low horizontal dFe flux estimates (21.5 µmol dFe m^{-2} d^{-1}; Milne et al., 2017).
553 Estimates of the vertical flux of dFe to the bottom of the SML were considerably lower than the
554 horizontal dFe fluxes on both the shelf (16 µmol m^{-2} d^{-1}) and the slope (0.024 to 0.043 µmol m^{-2} d^{-1})
555 (Figure 8; Milne et al., 2017). It is important to consider the speciation and redox state of the dFe that is
556 transported off the shelf, because Fe tends to form insoluble (oxy)hydroxides in the presence of oxygen
557 in seawater. In addition to Fe-ligand complexation, dFe may be stabilised in the presence of low oxygen
558 concentrations (> 45 µmol kg^{-1}; Figure 4) because oxidation of Fe(II) is slowed (Millero et al., 1987).
559 Although we have no measurements of Fe(II) in our samples, the Fe(II) content of Peru margin waters
560 with oxygen concentrations of > 50 µmol kg^{-1} was up to 20 % of the dFe pool (Chever et al., 2015). Hence,
561 it is likely that dFe in our OMZ samples partly consisted of Fe(II) derived from DIR. The Fe(II) half-life ($t_{1/2}$)
562 in bottom waters at station 4 and 5 was estimated to be ~ 30 to 70 min (using equations from Millero et
563 al., 1987, and [O_2] = 79 to 93 µmol kg^{-1}, T = 16 to 17 °C, Sal = 35.62 to 35.67, pH = 7.75 to 7.80).
564 Theoretical oxidation rates were slower in bottom waters at the slope Station 3, with Fe(II) $t_{1/2}$ ~ 325 min
565 ([O_2] = 130 µmol kg^{-1}, T = 5.4 °C, Sal = 34.84, pH = 7.81). Longer Fe(II) $t_{1/2}$ at this station may have
566 maintained the relatively high dFe concentrations supplied by sediment pore waters, and likely inhibited
567 the formation of Fe-(oxy)hydroxides. This is also supported by relatively high dFe concentrations within
568 the OMZ on the slope. Fe(II) oxidation was slowest in OMZ waters (Fe(II) $t_{1/2}$ ~500 min; stations 2 and 3),
569 which would facilitate offshore transport of a portion of shelf derived dFe. Since a shift towards lower
570 δ^{56}Fe values along potential Fe(II) oxidation pathways was not observed in this study, it is likely that as Fe
571 is gradually oxidised, part of it is immediately complexed to organic ligands or that hypothetical organic
572 ligand bound Fe(II) is gradually oxidised to its Fe(III) form (Klar et al., 2017a). Nonetheless, δ^{56}Fe values
573 imply that an important proportion of benthic dFe was supplied in the form of Fe(III) from NRD and
574 remineralisation, for which stabilisation with organic ligands plays a crucial role in terms of residence
575 time in the dissolved phase (Gledhill and Buck, 2012).

576 Benthic dFe inputs from shelf and slope sediments and, to a lesser extent at the time of our study,
577 atmospheric dFe inputs, therefore make an important contribution to the supply of “new” dFe to the
578 study area. Input of dFe from remineralisation of organic material also becomes an important source of
579 dFe within the OMZ with increasing distance from the shelf. We suggest that a considerable proportion
580 of the remineralised dFe is initially derived from benthic and (to a minor degree at the time of sampling)
581 atmospheric inputs in our study area. Our data provide a snapshot of part of a continuous cycle of
582 upwelling of high dFe bottom waters, biological uptake of this dFe, particle sinking and remineralisation,

583 the overall result of which is a shift from relatively low $\delta^{56}Fe$ values (dominated by benthic sedimentary
584 input of dFe) within the OMZ on the shelf towards higher $\delta^{56}Fe$ values (due to remineralisation of organic
585 material) within the OMZ further offshore (Figure 8). We envision that a significant part of sinking
586 organic material is not remineralised within the OMZ and is exported towards deeper waters, because
587 remineralisation rates may be low in OMZs (Cavan et al., 2017). Hence, the supply of new Fe (benthic
588 and atmospheric) must play an important role in maintaining the high dFe concentrations in the tropical
589 North Atlantic OMZ.

590 Our results are consistent with the conclusions of previous studies based on the analysis of dFe
591 concentrations, which inferred that remineralisation plays a key role in the supply of dFe to subsurface
592 waters of offshore regions of the tropical Atlantic OMZ (Rijkenberg et al., 2012; Fitzsimmons et al., 2013).
593 These studies observed a close correlation between dFe and AOU that indicated that the main dFe
594 source was from remineralisation of sinking material with a fixed Fe:C ratio. Rijkenberg et al. (2012)
595 observed a shift to higher Fe:C ratios north of 25 °N, indicative of shelf inputs. Accordingly, a study north
596 of the Cape Verde islands suggested that a shelf isotopic dFe signal can be observed up to 1000 km
597 outside the OMZ in the open ocean (with O_2 > 160 µmol kg^{-1}) (Conway and John, 2014). In their study,
598 the contribution of reduced dFe benthic inputs from the eastern margin to their ocean transect was
599 estimated using an end-member $\delta^{56}Fe$ value of -2.4 ‰ (as observed on the Californian margin, John et
600 al., 2012). We suggest that, due to the reactive nature of Fe in seawater, which is usually associated with
601 isotopic fractionation, mass-balance calculations based on Fe isotopes should be used with caution. In
602 addition, our data indicate that the $\delta^{56}Fe$ signal of dFe within the tropical Atlantic OMZ not only reflects
603 input of benthic Fe derived from DIR, but also benthic inputs of dFe from NRD and inputs of dFe from
604 remineralisation of organic material. Thus, the relatively higher $\delta^{56}Fe$ values observed in the eastern
605 Atlantic OMZ waters (this study and Conway and John et al., 2014) compared to those observed in
606 eastern Pacific OMZ waters (i.e., -1.3 to -0.3 ‰; (Chever et al., 2015; Fitzsimmons et al., 2016; John et al.,
607 2017) may be ultimately due to the larger annual input of atmospheric dust to the North Atlantic Ocean
608 and stronger overprinting of benthic signals from remineralisation in the Atlantic OMZ.

609 5. Conclusions

610 Our study confirms that remineralisation plays an important role in recycling dFe within the tropical
611 North Atlantic OMZ, but we also provide evidence for significant benthic inputs of dFe derived from both
612 DIR and NRD processes to low oxygen waters. At times of low atmospheric dust deposition, we suggest
613 that “new” Fe is mainly supplied by benthic inputs, and that consecutive cycles of bottom water

upwelling, biological uptake, and remineralisation of sinking organic matter lead to enhanced dFe concentrations in the eastern boundary tropical North Atlantic OMZ. These benthic inputs of dFe must be stabilised by complexation to organic ligands to allow offshore transport.

Regeneration of sinking organic material from the highly productive surface ocean is critical for maintaining high dFe concentrations within the tropical Atlantic OMZ, and upwelling transports these waters to the surface ocean. Since atmospheric dust deposition was low at the time of our study, but is known to be highly variable, the relative importance of new dFe delivered from atmospheric *versus* benthic inputs to the surface ocean of the tropical North Atlantic over the course of a year remains uncertain. However, because annual dust deposition is high in our study area compared to other parts of the ocean, NRD of lithogenic material in the water column and on the seafloor means that the isotopic composition of dFe is relatively high compared to other OMZs where levels of atmospheric dust deposition are lower.

With oxygen concentrations of seawater influencing remineralisation rates and Fe speciation, the decline in oceanic oxygen concentrations due to global warming may have significant consequences for Fe cycling. This needs to be investigated further and incorporated into future modelling efforts of the linkages between biogeochemical cycles and climate.

6. Acknowledgements

We gratefully acknowledge the support of the captain and crew of *RRS Discovery* throughout cruise D361. We also thank NMF staff for their technical assistance on-board. We thank the rest of the trace metal sampling team Maeve C Lohan, Angela Milne, Rosie Chance and Felix Morales for sharing the hard work on-board. We thank Eithne Tynan for pH data and Alexander Forryan for help with CTD data. We are grateful for the constructive comments from Olivier Rouxel and three anonymous reviewers, which have significantly improved this manuscript.

7. Funding

This study was funded by the UK National Environmental Research Council (NE/G015732/1) and the Atlantic Meridional Transect consortium (243). JKK's PhD studentship was funded by the Graduate School of the National Oceanography Centre and NERC National Capability Funds.

8. List of tables

9. List of figures

Figure 6: (a) Relationship between dFe and AOU and (b) relationship between $\delta^{56}Fe$ and remineralised dFe (dFe_{remin}) for the slope region (stations 2 and 3) between 100 and 1000 m depth. The average $\delta^{56}Fe$ value of the continental crust (+0.09 ± 0.10 ‰; Beard et al., 2003) is shown by the black line in (b). Linear regressions are shown by the dotted black lines.

Figure 7: Relationship between (a) $\delta^{56}Fe$ and dFe; and (b) $\delta^{56}Fe$ and O_2 on the shelf (stations 4 and 5) and on the slope (stations 2 and 3). The average $\delta^{56}Fe$ value of the continental crust (+0.09 ± 0.10 ‰; Beard et al., 2003) is shown by the horizontal black lines. Linear regressions of $\delta^{56}Fe$ *vs.* dFe for all samples and $\delta^{56}Fe$ *vs.* O_2 on the shelf are shown by the black dotted lines.

Figure 8: Schematic interpretation of the Fe cycle in our study area. Shelf sediments supply dFe with a light isotopic composition (↓ $\delta^{56}Fe$) to bottom waters. dFe is supplied to the surface mixed layer (SML) by atmospheric dust deposition and upwelled bottom waters, where phytoplankton takes up dFe with a relatively heavy isotopic composition (↑ $\delta^{56}Fe$). Remineralisation of sinking organic material leads to the release of dFe with a relatively heavy isotopic composition, which is mixed with benthic dFe inputs and upwelled to the SML, where it is mixed with atmospheric dFe inputs. The flux of benthic dFe decreases with distance from the coast. The continuous recycling of dFe by biological uptake and remineralisation leads to increasingly heavy isotopic compositions of dFe in the water column with distance from the shelf. Atmospheric dust inputs (fluxes in µmol dFe m^{-2} d^{-1}, in brown) to the SML, calculated from dAl concentrations, were low at the time of sampling but are potentially higher at other times of the year (Croot et al., 2004). Fluxes of vertical transport to the SML (white) and horizontal transport between the bottom of the SML and 500 m depth (yellow) are from Milne et al. (2017) and are in µmol dFe m^{-2} d^{-1}.

10. References

Abadie, C., Lacan, F., Radic, A., Pradoux, C. and Poitrasson, F. (2017) Iron isotopes reveal distinct dissolved iron sources and pathways in the intermediate versus deep Southern Ocean. *Proc. Natl. Acad. Sci.* **114**, 858-863.

Albarède, F. and Beard, B. (2004) Analytical methods for non-traditional isotopes, in: Johnson, C.M., Beard, B.L., Albarède, F. (Eds.), Geochemistry of Non-Traditional Stable Isotopes, pp. 113-152.

Beard, B.L., Johnson, C.M., Von Damm, K.L. and Poulson, R.L. (2003) Iron isotope constraints on Fe cycling and mass balance in oxygenated Earth oceans. *Geology* **31**, 629-632.

Bergquist, B.A. and Boyle, E.A. (2006) Iron isotopes in the Amazon River system: Weathering and transport signatures. *Earth. Planet. Sci. Lett.* **248**, 54-68.

Berman-Frank, I., Cullen, J.T., Shaked, Y., Sherrell, R.M. and Falkowski, P.G. (2001) Iron availability, cellular iron quotas, and nitrogen fixation in Trichodesmium. *Limnol. Oceanogr.* **46**, 1249-1260.

Boyd, P.W. and Ellwood, M.J. (2010) The biogeochemical cycle of iron in the ocean. *Nat. Geosci.* **3**, 675-682.

Boyle, E.A., John, S., Abouchami, W., Adkins, J.F., Echegoyen-Sanz, Y., Ellwood, M., Flegal, A.R., Fornace, K., Gallon, C., Galer, S., Gault-Ringold, M., Lacan, F., Radic, A., Rehkamper, M., Rouxel, O., Sohrin, Y., Stirling, C., Thompson, C., Vance, D., Xue, Z. and Zhao, Y. (2012) GEOTRACES IC1 (BATS) contamination-prone trace element isotopes Cd, Fe, Pb, Zn, Cu, and Mo intercalibration. *Limnol. Oceanogr. Meth.* **10**, 653-665.

Brandt, P., Hormann, V., Kortzinger, A., Visbeck, M., Krahmann, G., Stramma, L., Lumpkin, R. and Schmid, C. (2010) Changes in the Ventilation of the Oxygen Minimum Zone of the Tropical North Atlantic. *J. Phys. Oceanogr.* **40**, 1784-1801.

Broecker, W.S. (1974) Chemical oceanography. Harcourt Brace Jovanovich.

Brown, M.T. and Bruland, K.W. (2008) An improved flow-injection analysis method for the determination of dissolved aluminum in seawater. *Limnol. Oceanogr. Meth.* **6**, 87-95.

Buck, C.S., Landing, W.M., Resing, J.A. and Measures, C.I. (2010) The solubility and deposition of aerosol Fe and other trace elements in the North Atlantic Ocean: Observations from the A16N CLIVAR/CO(2) repeat hydrography section. *Mar. Chem.* **120**, 57-70.

719 Bullen, T.D., White, A.F., Childs, C.W., Vivit, D.V. and Schulz, M.S. (2001) Demonstration of significant
720 abiotic iron isotope fractionation in nature. *Geology* **29**, 699-702.

721 Burdige, D.J. (2006) Geochemistry of marine sediments. Princeton University Press, Princeton, NJ.

722 Canfield, D.E. (1989) Reactive iron in marine sediments. *Geochim. Cosmochim. Acta* **53**, 619-632.

723 Carpenter, J.H. (1965) The accuracy of the Winkler method for dissolved oxygen analysis. *Limnol.*
724 *Oceanogr.* **10**, 135-140.

725 Cavan, E.L., Trimmer, M., Shelley, F. and Sanders, R. (2017) Remineralization of particulate organic
726 carbon in an ocean oxygen minimum zone. *Nat. Commun.* **8**, 14847.

727 Chan, F., Barth, J.A., Lubchenco, J., Kirincich, A., Weeks, H., Peterson, W.T. and Menge, B.A. (2008)
728 Emergence of anoxia in the California current large marine ecosystem. *Science* **319**, 920-920.

729 Chever, F., Rouxel, O.J., Croot, P.L., Ponzevera, E., Wuttig, K. and Auro, M. (2015) Total dissolvable and
730 dissolved iron isotopes in the water column of the Peru upwelling regime. *Geochim. Cosmochim. Acta*
731 **162**, 66-82.

732 Coale, K.H., Johnson, K.S., Chavez, F.P., Buesseler, K.O., Barber, R.T., Brzezinski, M.A., Cochlan, W.P.,
733 Millero, F.J., Falkowski, P.G., Bauer, J.E., Wanninkhof, R.H., Kudela, R.M., Altabet, M.A., Hales, B.E.,
734 Takahashi, T., Landry, M.R., Bidigare, R.R., Wang, X.J., Chase, Z., Strutton, P.G., Friederich, G.E.,
735 Gorbunov, M.Y., Lance, V.P., Hilting, A.K., Hiscock, M.R., Demarest, M., Hiscock, W.T., Sullivan, K.F.,
736 Tanner, S.J., Gordon, R.M., Hunter, C.N., Elrod, V.A., Fitzwater, S.E., Jones, J.L., Tozzi, S., Koblizek, M.,
737 Roberts, A.E., Herndon, J., Brewster, J., Ladizinsky, N., Smith, G., Cooper, D., Timothy, D., Brown, S.L.,
738 Selph, K.E., Sheridan, C.C., Twining, B.S. and Johnson, Z.I. (2004) Southern ocean iron enrichment
739 experiment: Carbon cycling in high- and low-Si waters. *Science* **304**, 408-414.

740 Conway, T.M. and John, S.G. (2014) Quantification of dissolved iron sources to the North Atlantic Ocean.
741 *Nature* **511**, 13482.

742 Conway, T.M., John, S.G. and Lacan, F. (2016) Intercomparison of dissolved iron isotope profiles from
743 reoccupation of three GEOTRACES stations in the Atlantic Ocean. *Mar. Chem.* **183**, 50-61.

744 Conway, T.M., Rosenberg, A.D., Adkins, J.F. and John, S.G. (2013) A new method for precise
745 determination of iron, zinc and cadmium stable isotope ratios in seawater by double-spike mass
746 spectrometry. *Anal. Chim. Acta* **793**, 44-52.

747 Croot, P.L., Streu, P. and Baker, A.R. (2004) Short residence time for iron in surface seawater impacted by
748 atmospheric dry deposition from Saharan dust events. *Geophys. Res. Lett.* **31**, L23S08.

749 Dammshäuser, A., Wagener, T. and Croot, P.L. (2011) Surface water dissolved aluminum and titanium:
750 Tracers for specific time scales of dust deposition to the Atlantic? *Geophys. Res. Lett.* **38**, L24601.

751 Dauphas, N., Pourmand, A. and Teng, F.Z. (2009) Routine isotopic analysis of iron by HR-MC-ICPMS: How
752 precise and how accurate? *Chem. Geol.* **267**, 175-184.

753 Dauphas, N. and Rouxel, O. (2006) Mass spectrometry and natural variations of iron isotopes. *Mass*
754 *Spectrom. Rev.* **25**, 515-550.

755 Dideriksen, K., Baker, J.A. and Stipp, S.L.S. (2008) Equilibrium Fe isotope fractionation between inorganic
756 aqueous Fe(III) and the siderophore complex, Fe(III)-desferrioxamine B. *Earth. Planet. Sci. Lett.* **269**, 280-
757 290.

758 Ellwood, M.J., Hutchins, D.A., Lohan, M.C., Milne, A., Nasemann, P., Nodder, S.D., Sander, S.G., Strzepek,
759 R., Wilhelm, S.W. and Boyd, P.W. (2015) Iron stable isotopes track pelagic iron cycling during a
760 subtropical phytoplankton bloom. *Proc. Natl. Acad. Sci.* **112**, E15-E20.

761 Eppley, R.W. and Peterson, B.J. (1979) Particulate organic matter flux and planktonic new production in
762 the deep ocean. *Nature* **282**, 677.

763 Escoube, R., Rouxel, O.J., Pokrovsky, O.S., Schroth, A., Max Holmes, R. and Donard, O.F.X. (2015) Iron
764 isotope systematics in Arctic rivers. *C. R. Geosci.* **347**, 377-385.

765 Escoube, R., Rouxel, O.J., Sholkovitz, E. and Donard, O.F.X. (2009) Iron isotope systematics in estuaries:
766 The case of North River, Massachusetts (USA). *Geochim. Cosmochim. Acta* **73**, 4045-4059.

767 Falkowski, P.G. (1997) Evolution of the nitrogen cycle and its influence on the biological sequestration of
768 CO2 in the ocean. *Nature* **387**, 272-275.

769 Fitzsimmons, J.N., Conway, T.M., Lee, J.M., Kayser, R., Thyng, K.M., John, S.G. and Boyle, E.A. (2016)
770 Dissolved iron and iron isotopes in the southeastern Pacific Ocean. *Global Biogeochem. Cycles* **30**, 1372-
771 1395.

772 Fitzsimmons, J.N., Zhang, R. and Boyle, E.A. (2013) Dissolved iron in the tropical North Atlantic Ocean.
773 *Mar. Chem.* **154**, 87-99.

774 Gehlen, M., Beck, L., Calas, G., Flank, A.M., Van Bennekom, A.J. and Van Beusekom, J.E.E. (2002)
775 Unraveling the atomic structure of biogenic silica: Evidence of the structural association of Al and Si in
776 diatom frustules. *Geochim. Cosmochim. Acta* **66**, 1601-1609.

777 Gledhill, M. and Buck, K.N. (2012) The organic complexation of iron in the marine environment: a review.
778 *Front Microbiol.* **3**.

779 Goldberg, E.D. (1954) Marine Geochemistry 1. Chemical Scavengers of the Sea. *The Journal of Geology*
780 **62**, 249-265.

781 Henkel, S., Kasten, S., Poulton, S.W. and Staubwasser, M. (2016) Determination of the stable iron
782 isotopic composition of sequentially leached iron phases in marine sediments. *Chem. Geol.* **421**, 93-102.

783 Hioki, N., Kuma, K., Morita, Y., Sasayama, R., Ooki, A., Kondo, Y., Obata, H., Nishioka, J., Yamashita, Y.,
784 Nishino, S., Kikuchi, T. and Aoyama, M. (2014) Laterally spreading iron, humic-like dissolved organic
785 matter and nutrients in cold, dense subsurface water of the Arctic Ocean. *Sci. Rep.* **4**, 6775.

786 Homoky, W.B., John, S.G., Conway, T.M. and Mills, R.A. (2013) Distinct iron isotopic signatures and
787 supply from marine sediment dissolution. *Nat. Commun.* **4**.

788 Homoky, W.B., Severmann, S., Mills, R.A., Statham, P.J. and Fones, G.R. (2009) Pore-fluid Fe isotopes
789 reflect the extent of benthic Fe redox recycling: Evidence from continental shelf and deep-sea sediments.
790 *Geology* **37**, 751-754.

791 Jickells, T.D., An, Z.S., Andersen, K.K., Baker, A.R., Bergametti, G., Brooks, N., Cao, J.J., Boyd, P.W., Duce,
792 R.A., Hunter, K.A., Kawahata, H., Kubilay, N., laRoche, J., Liss, P.S., Mahowald, N., Prospero, J.M.,
793 Ridgwell, A.J., Tegen, I. and Torres, R. (2005) Global iron connections between desert dust, ocean
794 biogeochemistry, and climate. *Science* **308**, 67-71.

795 Jickells, T.D., Baker, A.R. and Chance, R. (2016) Atmospheric transport of trace elements and nutrients to
796 the oceans. *Philosophical Transactions of the Royal Society A: Mathematical Physical and Engineering*
797 *Sciences* **374**.

798 John, S.G. and Adkins, J. (2012) The vertical distribution of iron stable isotopes in the North Atlantic near
799 Bermuda. *Global Biogeochem. Cycles* **26**.

800 John, S.G. and Adkins, J.F. (2010) Analysis of dissolved iron isotopes in seawater. *Mar. Chem.* **119**, 65-76.

801 John, S.G., Helgoe, J., Townsend, E., Weber, T., DeVries, T., Tagliabue, A., Moore, K., Lam, P., Marsay,
802 C.M. and Till, C. (2017) Biogeochemical cycling of Fe and Fe stable isotopes in the Eastern Tropical South
803 Pacific. *Mar. Chem.*

804 John, S.G., Mendez, J., Moffett, J. and Adkins, J. (2012) The flux of iron and iron isotopes from San Pedro
805 Basin sediments. *Geochim. Cosmochim. Acta* **93**, 14-29.

806 Jones, M.E., Beckler, J.S. and Taillefert, M. (2011) The flux of soluble organic-iron(III) complexes from
807 sediments represents a source of stable iron(III) to estuarine waters and to the continental shelf. *Limnol.*
808 *Oceanogr.* **56**, 1811-1823.

809 Karstensen, J., Stramma, L. and Visbeck, M. (2008) Oxygen minimum zones in the eastern tropical
810 Atlantic and Pacific oceans. *Prog. Oceanogr.* **77**, 331-350.

811 Keeling, R.F., Koertzinger, A. and Gruber, N. (2010) Ocean Deoxygenation in a Warming World. *Annu.*
812 *Rev. Mar. Sci* **2**, 199-229.

813 Klar, J.K., Homoky, W.B., Statham, P.J., Birchill, A.J., Harris, E.L., Woodward, E.M.S., Silburn, B., Cooper,
814 M.J., James, R.H., Connelly, D.P., Chever, F., Lichtschlag, A. and Graves, C. (2017a) Stability of dissolved
815 and soluble Fe(II) in shelf sediment pore waters and release to an oxic water column. *Biogeochemistry*
816 **135**, 49-67.

817 Klar, J.K., James, R.H., Gibbs, D., Lough, A., Parkinson, I., Milton, J.A., Hawkes, J.A. and Connelly, D.P.
818 (2017b) Isotopic signature of dissolved iron delivered to the Southern Ocean from hydrothermal vents in
819 the East Scotia Sea. *Geology* **45**, 351-354.

820 Klunder, M.B., Laan, P., Middag, R., de Baar, H.J.W. and Bakker, K. (2012) Dissolved iron in the Arctic
821 Ocean: Important role of hydrothermal sources, shelf input and scavenging removal. *J. Geophys. Res.-*
822 *Oceans* **117**, C04014.

823 Klunder, M.B., Laan, P., Middag, R., De Baar, H.J.W. and van Ooijen, J.C. (2011) Dissolved iron in the
824 Southern Ocean (Atlantic sector). *Deep Sea Res. Pt. II* **58**, 2678-2694.

825 Kramer, J., Laan, P., Sarthou, G., Timmermans, K.R. and de Baar, H.J.W. (2004) Distribution of dissolved
826 aluminium in the high atmospheric input region of the subtropical waters of the North Atlantic Ocean.
827 *Mar. Chem.* **88**, 85-101.

828 Labatut, M., Lacan, F., Pradoux, C., Chmeleff, J., Radic, A., Murray, J.W., Poitrasson, F., Johansen, A.M.
829 and Thil, F. (2014) Iron sources and dissolved-particulate interactions in the seawater of the Western
830 Equatorial Pacific, iron isotope perspectives. *Global Biogeochem. Cycles* **28**, 1044-1065.

831 Lacan, F., Radic, A., Jeandel, C., Poitrasson, F., Sarthou, G., Pradoux, C. and Freydier, R. (2008)
832 Measurement of the isotopic composition of dissolved iron in the open ocean. *Geophys. Res. Lett.* **35**,
833 L24610.

834 Lacan, F., Radic, A., Labatut, M., Jeandel, C., Poitrasson, F., Sarthou, G., Pradoux, C., Chmeleff, J. and
835 Freydier, R. (2010) High-Precision Determination of the Isotopic Composition of Dissolved Iron in Iron
836 Depleted Seawater by Double Spike Multicollector-ICPMS. *Anal. Chem.* **82**, 7103-7111.

837 Le Quéré, C., Andres, R.J., Boden, T., Conway, T., Houghton, R.A., House, J.I., Marland, G., Peters, G.P.,
838 van der Werf, G.R., Ahlström, A., Andrew, R.M., Bopp, L., Canadell, J.G., Ciais, P., Doney, S.C., Enright, C.,
839 Friedlingstein, P., Huntingford, C., Jain, A.K., Jourdain, C., Kato, E., Keeling, R.F., Klein Goldewijk, K., Levis,
840 S., Levy, P., Lomas, M., Poulter, B., Raupach, M.R., Schwinger, J., Sitch, S., Stocker, B.D., Viovy, N., Zaehle,
841 S. and Zeng, N. (2013) The global carbon budget 1959–2011. *Earth Syst. Sci. Data* **5**, 165-185.

842 Liu, X. and Millero, F.J. (2002) The solubility of iron in seawater. *Mar. Chem.* **77**, 43-54.

843 Lomnitz, U. (2017) Biogeochemical cycling of iron and phosphorus under low oxygen conditions,
844 Mathematisch-Naturwissenschaftliche Fakultät. Ph. D. Thesis, Christian-Albrechts-Universität zu Kiel,
845 Kiel.

846 Mackey, D.J., O'Sullivan, J.E.O. and Watson, R.J. (2002) Iron in the western Pacific: a riverine or
847 hydrothermal source for iron in the Equatorial Undercurrent? *Deep Sea Res. Pt. I* **49**, 877-893.

848 Marsay, C.M., Sedwick, P.N., Dinniman, M.S., Barrett, P.M., Mack, S.L. and McGillicuddy, D.J. (2014)
849 Estimating the benthic efflux of dissolved iron on the Ross Sea continental shelf. *Geophys. Res. Lett.* **41**,
850 7576-7583.

851 Martin, J.H. (1990) Glacial-interglacial CO2 change: the iron hypothesis. *Paleoceanography* **5**, 1-13.

852 Martin, J.H. and Fitzwater, S.E. (1988) Iron-deficiency limits phytoplankton growth in the northeast
853 Pacific Subarctic. *Nature* **331**, 341-343.

854 Martin, J.H., Knauer, G.A., Karl, D.M. and Broenkow, W.W. (1987) VERTEX: carbon cycling in the
855 northeast Pacific. *Deep Sea Res. Pt. I* **34**, 267-285.

856 Mead, C., Herckes, P., Majestic, B.J. and Anbar, A.D. (2013) Source apportionment of aerosol iron in the
857 marine environment using iron isotope analysis. *Geophys. Res. Lett.* **40**, 5722-5727.

858 Measures, C.I. and Brown, E.T. (1996) Estimating dust input to the Atlantic Ocean using surface water Al
859 concentrations, in: Guerzoni, S., Chester, R. (Eds.), The Impact of Desert Dust Across the Mediterranean.
860 Kluwer Academic Publishers, Dortrecht, p. 389.

861 Millero, F.J., Sotolongo, S. and Izaguirre, M. (1987) The oxidation-kinetics of Fe(II) in seawater. *Geochim.*
862 *Cosmochim. Acta* **51**, 793-801.

863 Milne, A., Schlosser, C., Wake, B.D., Achterberg, E.P., Chance, R., Baker, A.R., Forryan, A. and Lohan, M.C.
864 (2017) Particulate phases are key in controlling dissolved iron concentrations in the (sub)tropical North
865 Atlantic. *Geophys. Res. Lett.* **44**, 2377-2387.

866 Monterey, G.I. and Levitus, S. (1997) Seasonal variability of mixed layer depth for the world ocean. US
867 Department of Commerce, National Oceanic and Atmospheric Administration, National Environmental
868 Satellite, Data, and Information Service.

869 Moore, J.K., Doney, S.C., Glover, D.M. and Fung, I.Y. (2002) Iron cycling and nutrient-limitation patterns
870 in surface waters of the World Ocean. *Deep Sea Res. Pt. II* **49**, 463-507.

871 Moran, S.B. and Moore, R.M. (1992) Kinetics of the removal of dissolved aluminum by diatoms in
872 seawater: A comparison with thorium. *Geochim. Cosmochim. Acta* **56**, 3365-3374.

873 Morgan, J.L.L., Wasylenki, L.E., Nuester, J. and Anbar, A.D. (2010) Fe Isotope Fractionation during
874 Equilibration of Fe-Organic Complexes. *Environ. Sci. Technol.* **44**, 6095-6101.

875 Nishioka, J. and Obata, H. (2017) Dissolved iron distribution in the western and central subarctic Pacific:
876 HNLC water formation and biogeochemical processes. *Limnol. Oceanogr.* **62**, 2004-2022.

877 Noffke, A., Hensen, C., Sommer, S., Scholz, F., Bohlen, L., Mosch, T., Graco, M. and Wallmann, K. (2012)
878 Benthic iron and phosphorus fluxes across the Peruvian oxygen minimum zone. *Limnol. Oceanogr.* **57**,
879 851-867.

880 Patey, M.D., Achterberg, E.P., Rijkenberg, M.J. and Pearce, R. (2015) Aerosol time-series measurements
881 over the tropical Northeast Atlantic Ocean: Dust sources, elemental composition and mineralogy. *Mar.*
882 *Chem.* **174**, 103-119.

883 Planquette, H., Statham, P.J., Fones, G.R., Charette, M.A., Moore, C.M., Salter, I., Nedelec, F.H., Taylor,
884 S.L., French, M., Baker, A.R., Mahowald, N. and Jickells, T.D. (2007) Dissolved iron in the vicinity of the
885 Crozet Islands, Southern Ocean. *Deep-Sea Res. Pt. II* **54**, 1999-2019.

886 Radic, A., Lacan, F. and Murray, J.W. (2011) Iron isotopes in the seawater of the equatorial Pacific Ocean:
887 New constraints for the oceanic iron cycle. *Earth. Planet. Sci. Lett.* **306**, 1-10.

888 Resing, J.A. and Measures, C.I. (1994) Fluorometric determination of Al in seawater by Flow-Injection-
889 Analysis with in-line preconcentration. *Anal. Chem.* **66**, 4105-4111.

890 Resing, J.A., Sedwick, P.N., German, C.R., Jenkins, W.J., Moffett, J.W., Sohst, B.M. and Tagliabue, A.
891 (2015) Basin-scale transport of hydrothermal dissolved metals across the South Pacific Ocean. *Nature*
892 **523**, 200-203.

Rijkenberg, M.J.A., Middag, R., Laan, P., Gerringa, L.J.A., van Aken, H.M., Schoemann, V., de Jong, J.T.M. and de Baar, H.J.W. (2014) The distribution of dissolved iron in the west atlantic ocean. *PloS one* **9**, e101323.

Rijkenberg, M.J.A., Steigenberger, S., Powell, C.F., van Haren, H., Patey, M.D., Baker, A.R. and Achterberg, E.P. (2012) Fluxes and distribution of dissolved iron in the eastern (sub-) tropical North Atlantic Ocean. *Global Biogeochem. Cycles* **26**, GB3004.

Rouxel, O., Shanks, W.C., Bach, W. and Edwards, K.J. (2008) Integrated Fe- and S-isotope study of seafloor hydrothermal vents at East Pacific rise 9-10 degrees N. *Chem. Geol.* **252**, 214-227.

Schlosser, C., Klar, J.K., Wake, B.D., Snow, J.T., Honey, D.J., Woodward, E.M.S., Lohan, M.C., Achterberg, E.P. and Moore, C.M. (2014) Seasonal ITCZ migration dynamically controls the location of the (sub)tropical Atlantic biogeochemical divide. *Proc. Natl. Acad. Sci.* **111**, 1438-1442.

Schmidtko, S., Stramma, L. and Visbeck, M. (2017) Decline in global oceanic oxygen content during the past five decades. *Nature* **542**, 335-339.

Scholz, F., Severmann, S., McManus, J. and Hensen, C. (2014) Beyond the Black Sea paradigm: The sedimentary fingerprint of an open-marine iron shuttle. *Geochim. Cosmochim. Acta* **127**, 368-380.

Schott, F.A., McCreary, J.P. and Johnson, G.C. (2004) Shallow Overturning Circulations of the Tropical-Subtropical Oceans, Earth's Climate. American Geophysical Union, pp. 261-304.

Severmann, S., Johnson, C.M., Beard, B.L. and McManus, J. (2006) The effect of early diagenesis on the Fe isotope compositions of porewaters and authigenic minerals in continental margin sediments. *Geochim. Cosmochim. Acta* **70**, 2006-2022.

Severmann, S., McManus, J., Berelson, W.M. and Hammond, D.E. (2010) The continental shelf benthic iron flux and its isotope composition. *Geochim. Cosmochim. Acta* **74**, 3984-4004.

915 Siedlecki, S.A., Mahadevan, A. and Archer, D.E. (2012) Mechanism for export of sediment-derived iron in
916 an upwelling regime. *Geophys. Res. Lett.* **39**, L03601.

917 Siedler, G., Kuhl, A. and Zenk, W. (1987) The Madeira mode water. *J. Phys. Oceanogr.* **17**, 1561-1570.

918 Stramma, L., Brandt, P., Schafstall, J., Schott, F., Fischer, J. and Koertzinger, A. (2008a) Oxygen minimum
919 zone in the North Atlantic south and east of the Cape Verde Islands. *J. Geophys. Res.-Oceans* **113**,
920 L03601.

921 Stramma, L. and England, M. (1999) On the water masses and mean circulation of the South Atlantic
922 Ocean. *Journal of Geophysical Research: Oceans* **104**, 20863-20883.

923 Stramma, L., Huttl, S. and Schafstall, J. (2005) Water masses and currents in the upper tropical northeast
924 Atlantic off northwest Africa. *J. Geophys. Res.-Oceans* **110**, C12006.

925 Stramma, L., Johnson, G.C., Sprintall, J. and Mohrholz, V. (2008b) Expanding oxygen-minimum zones in
926 the tropical oceans. *Science* **320**, 655-658.

927 Stramma, L. and Schott, F. (1999) The mean flow field of the tropical Atlantic Ocean. *Deep-Sea Res. Pt. II*
928 **46**, 279-303.

929 Tagliabue, A., Bowie, A.R., Boyd, P.W., Buck, K.N., Johnson, K.S. and Saito, M.A. (2017) The integral role
930 of iron in ocean biogeochemistry. *Nature* **543**, 51-59.

931 Taylor, S.R. (1964) Abundance of chemical elements in the continental crust: a new table. *Geochim.*
932 *Cosmochim. Acta* **28**, 1273-1285.

933 Twining, B.S., Rauschenberg, S., Morton, P.L. and Vogt, S. (2015) Metal contents of phytoplankton and
934 labile particulate material in the North Atlantic Ocean. *Prog. Oceanogr.* **137, Part A**, 261-283.

935 Ussher, S.J., Achterberg, E.P., Powell, C., Baker, A.R., Jickells, T.D., Torres, R. and Worsfold, P.J. (2013)
936 Impact of atmospheric deposition on the contrasting iron biogeochemistry of the North and South
937 Atlantic Ocean. *Global Biogeochem. Cycles* **27**, 1096-1107.

938 Ussher, S.J., Achterberg, E.P., Sarthou, G., Laan, P., de Baar, H.J.W. and Worsfold, P.J. (2010) Distribution
939 of size fractionated dissolved iron in the Canary Basin. *Mar. Environ. Res.* **70**, 46-55.

940 Ussher, S.J., Achterberg, E.P. and Worsfold, P.J. (2004) Marine Biogeochemistry of Iron. *Environ. Chem.* **1**,
941 67-80.

942 Waeles, M., Baker, A.R., Jickells, T. and Hoogewerff, J. (2007) Global dust teleconnections: aerosol iron
943 solubility and stable isotope composition. *Environ. Chem.* **4**, 233-237.

944 Woodward, E.M.S. and Rees, A.P. (2001) Nutrient distributions in an anticyclonic eddy in the northeast
945 Atlantic Ocean, with reference to nanomolar ammonium concentrations. *Deep-Sea Res. Pt. II* **48**, 775-
946 793.

947

948

Table 1

Sample ID	Depth (m)	σ_θ (kg m^{-3})	Oxygen (µmol kg^{-1})	Salinity	pot T (°C)	water mass	dFe (nmol L^{-1})	2 SD (nmol L^{-1})	δ^{56}Fe (‰)	2 SD (‰)	Phosphate (µmol L^{-1})	Nitrate (µmol L^{-1})
Station 4, Cast 11, 12.6120 N, -17.5728 E, 51 m bottom depth												
11_12	25	25.66	158.5	35.71	18.61	TSW	2.5	0.2	0.03	0.04	0.97	13.51
11_11	38	25.79	119.8	35.69	18.01	TSW	3.36	0.08	-0.20	0.04	1.08	15.76
11_10	40	25.83	111.6	35.68	17.84	TSW	3.49	0.16	-0.32	0.04	1.12	16.14
11_09	49	25.91	93.1	35.67	17.48	SACW	3.82	0.06	-0.25	0.04	1.13	6.68
Station 5, Cast 12, 12.5882 N, -17.5724 E, 164 m bottom depth												
12_23	26	25.72	138.4	35.69	18.34	TSW	3.01	0.10	-0.11	0.05	1.10	15.48
12_21	36	25.79	116.8	35.68	18.01	TSW	2.99	0.13	-0.23	0.05	1.21	17.26
12_19	51	25.88	96.9	35.67	17.63	SACW	3.5	0.2	-0.16	0.05	1.25	18.03
12_17	66	25.93	81.2	35.66	17.37	SACW	3.75	0.06	-0.25	0.04	1.25	18.08
12_15	80	25.96	78.5	35.66	17.23	SACW	3.68	0.09	-0.31	0.05	1.29	18.89
12_13	107	26.18	68.8	35.62	16.22	SACW	6.3	0.5	-0.33	0.05	1.43	21.51
Station 3, Cast 8, 12.6100 N, -17.7157 E, 1041 m bottom depth												
8_21	199	26.54	71.9	35.44	13.94	SACW	1.81	0.02	0.06	0.08	1.59	25.63
8_20	300	26.85	59.3	35.39	12.22	SACW	2.58	0.02	-0.15	0.08	1.73	28.62
8_19	400	27.03	44.6	35.27	10.76	SACW	2.86	0.08	-0.19	0.04	1.98	32.82
8_18	500	27.14	48.9	35.10	9.38	SACW/AAIW	3.77	0.19	-0.32	0.04	2.17	34.79
8_17	599	27.21	60.1	34.89	7.83	AAIW	2.14	0.09	-0.08	0.04	2.33	36.72
8_16	699	27.28	74.0	34.84	7.08	AAIW	2.66	0.05	-0.30	0.04	1.91	30.81
8_14	899	27.38	99.5	34.79	6.06	AAIW	2.69	0.06	-0.26	0.04	2.32	34.88
8_13	1002	27.50	130.8	34.84	5.38	AAIW	2.90	0.18	-0.27	0.04	2.16	31.77
									-0.21	0.08		

Station 2, Cast 6, 12.5942 N, -17.9199 E, 2656 m bottom depth												
6_21	198	26.63	70.5	35.41	13.39	SACW	1.85	0.10	-0.06	0.08	1.62	26.69
6_20	299	26.86	58.1	35.38	12.07	SACW	1.89	0.05	0.02	0.08	1.81	30.37
6_19	399	27.03	43.8	35.27	10.75	SACW	1.51	0.08	0.21	0.04	1.98	33.18
6_18	499	27.14	49.7	35.14	9.52	SACW/AAIW	1.40	0.04	0.41	0.04	2.19	35.37
6_17	599	27.22	58.5	34.93	7.93	AAIW	1.96	0.06	0.10	0.08	2.32	36.89
6_16	750	27.32	85.0	34.78	6.46	AAIW	1.82	0.05	0.12	0.08	2.37	36.55
									0.12	0.05		
6_15	900	27.40	111.1	34.76	5.64	AAIW	1.74	0.05	0.09	0.08	2.32	34.61
6_12	1699	27.77	216.9	34.96	3.82	NADW	1.66	0.03	0.12	0.08	1.60	22.76
6_10	2625	27.86	237.6	34.94	2.77	NADW	1.33	0.03	0.09	0.04	1.56	21.18

Table 2

Sample ID	Lat (°N)	Long (°E)	Stn	SMLD (m)	dAl_{meas} (nmol L^{-1})	SD	dFe_{meas} (nmol L^{-1})	SD	dust flux (g dust m^{-2} y^{-1})	SD	dust flux (µmol dFe m^{-2} d^{-1})	SD	dFe_{dust} (nmol L^{-1})	SD
F-44	12.590	-17.653	4 & 5	11	0.9	0.4	0.48	0.03	0.02	0.02	0.002	0.002	0.05	0.06
F-45	12.587	-17.714	3	19	2.1	0.4	0.45	0.02	0.08	0.07	0.009	0.009	0.12	0.13
F-46	12.586	-17.773		11	1.0	0.4			0.02	0.02	0.003	0.003	0.06	0.07
F-47	12.586	-17.831		11	2.4	0.4	0.76	0.02	0.05	0.05	0.006	0.006	0.14	0.14
F-48	12.585	-17.890	2	11	1.1	0.4	0.73	0.09	0.02	0.02	0.003	0.003	0.07	0.07
F-49	12.585	-17.949		11	2.1	0.4	0.83	0.03	0.05	0.04	0.005	0.005	0.12	0.13
			shelf								0.075*		1.74	
			slope								0.074*		1.72	

* Data from Milne et al., 2017

Figure 1

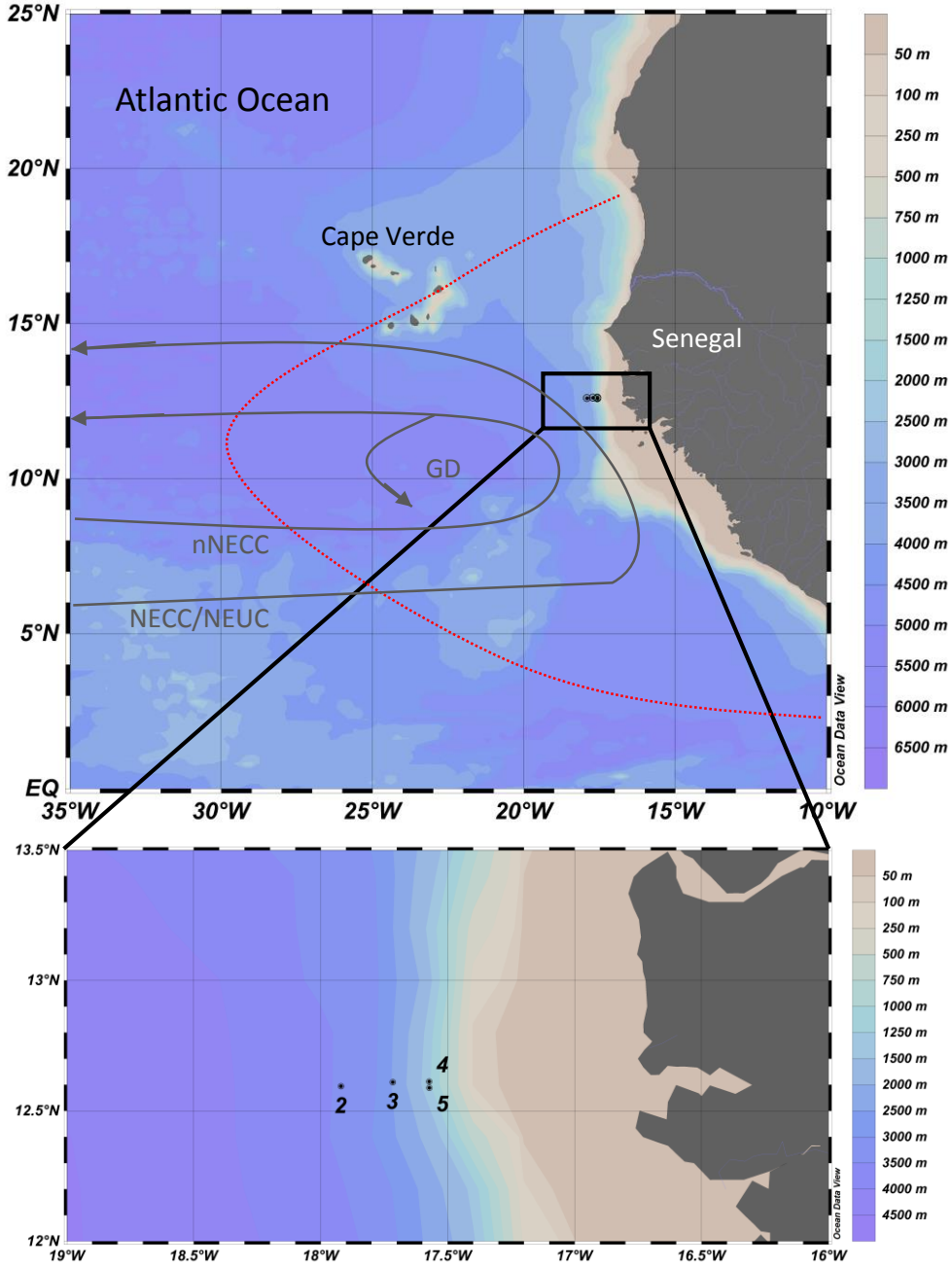
Atlantic Ocean
Cape Verde
Senegal
GD
nNECC
NECC/NEUC
25°N
20°N
15°N
10°N
5°N
EQ
35°W
30°W
25°W
20°W
15°W
10°W
50 m
100 m
250 m
500 m
750 m
1000 m
1250 m
1500 m
2000 m
2500 m
3000 m
3500 m
4000 m
4500 m
5000 m
5500 m
6000 m
6500 m
Ocean Data View
13.5°N
13°N
12.5°N
12°N
19°W
18.5°W
18°W
17.5°W
17°W
16.5°W
16°W
2
3
4
5

Figure 2

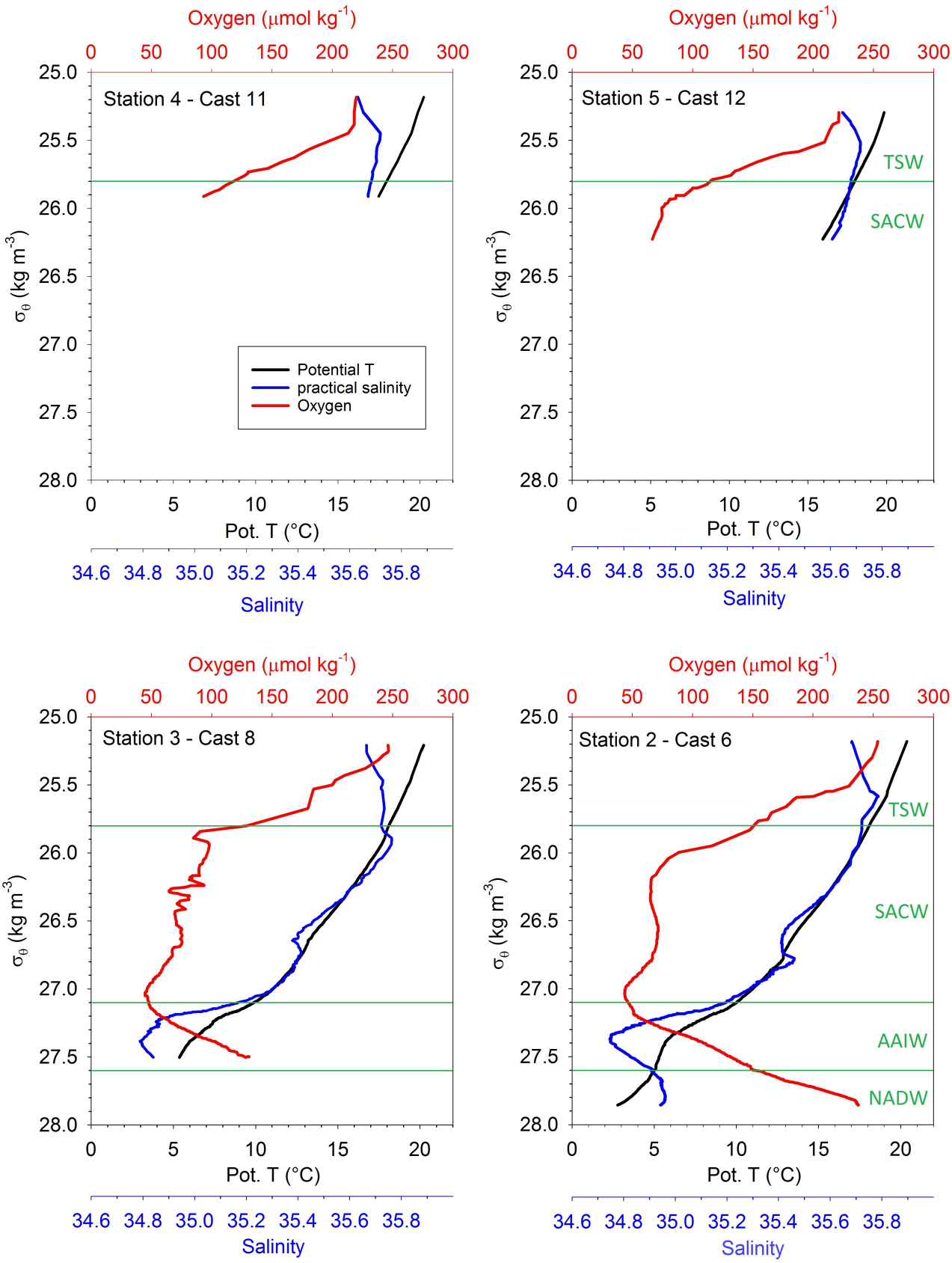
Oxygen (µmol kg-1)
0 50 100 150 200 250 300
Station 4 - Cast 11
Station 5 - Cast 12
Station 3 - Cast 8
Station 2 - Cast 6
TSW
SACW
AAIW
NADW
σθ (kg m-3)
25.0 25.5 26.0 26.5 27.0 27.5 28.0
Potential T
practical salinity
Oxygen
0 5 10 15 20
Pot. T (°C)
34.6 34.8 35.0 35.2 35.4 35.6 35.8
Salinity

Figure 3

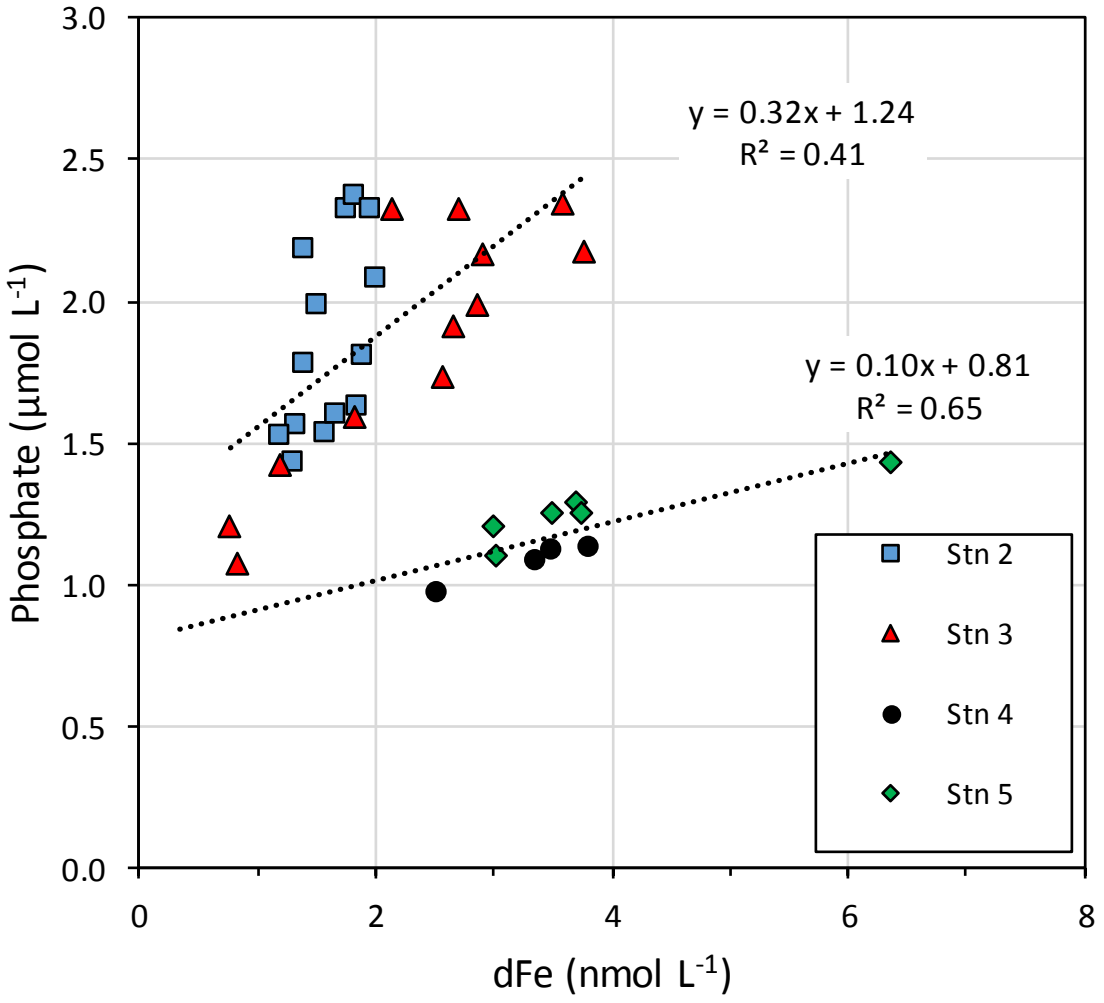
y = 0.32x + 1.24
R² = 0.41
y = 0.10x + 0.81
R² = 0.65
Stn 2
Stn 3
Stn 4
Stn 5
Phosphate (µmol L-1)
dFe (nmol L-1)
0.0
0.5
1.0
1.5
2.0
2.5
3.0
0
2
4
6
8

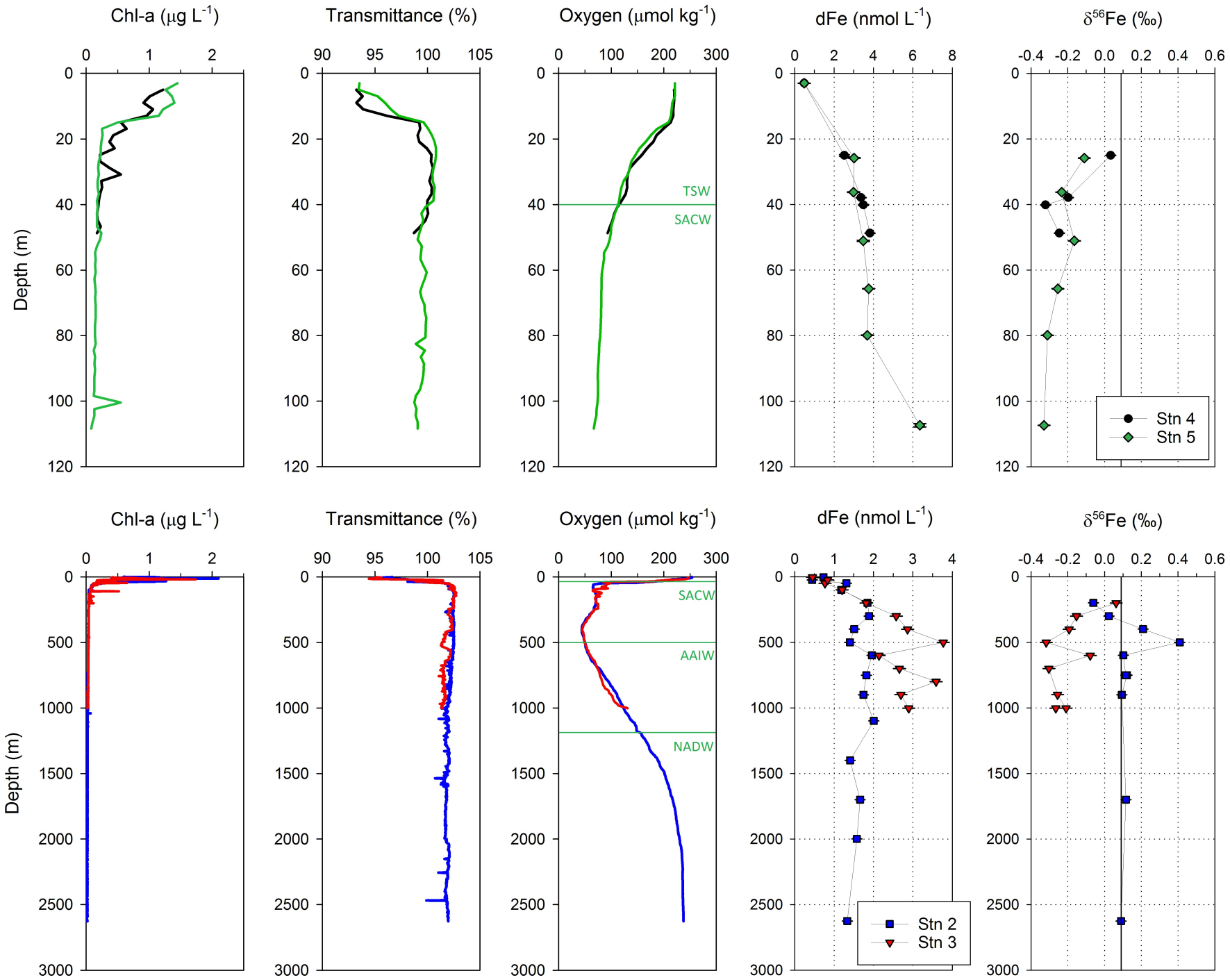
Chl-a (μg L-1)
Transmittance (%)
Oxygen (μmol kg-1)
dFe (nmol L-1)
δ56Fe (‰)
Depth (m)
TSW
SACW
Stn 4
Stn 5
AAIW
NADW
Stn 2
Stn 3

Figure 4

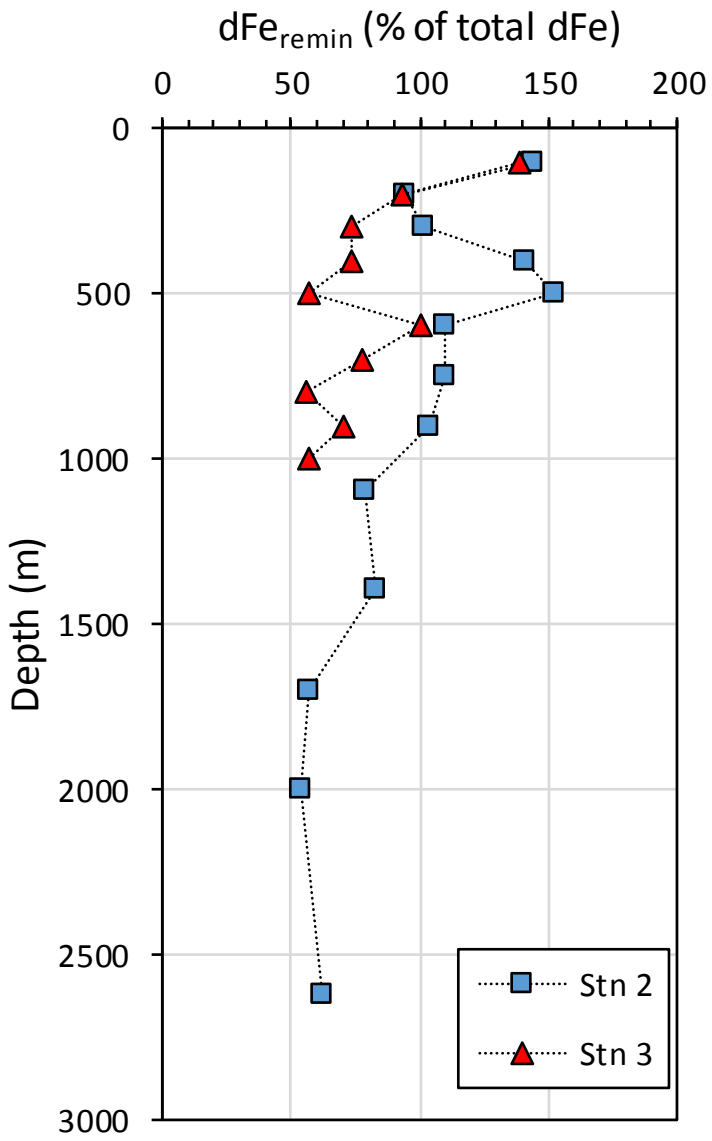
dFe$_{remin}$ (% of total dFe)
0
50
100
150
200
0
500
1000
1500
2000
2500
3000
Depth (m)
Stn 2
Stn 3

Figure 5

Figure 6

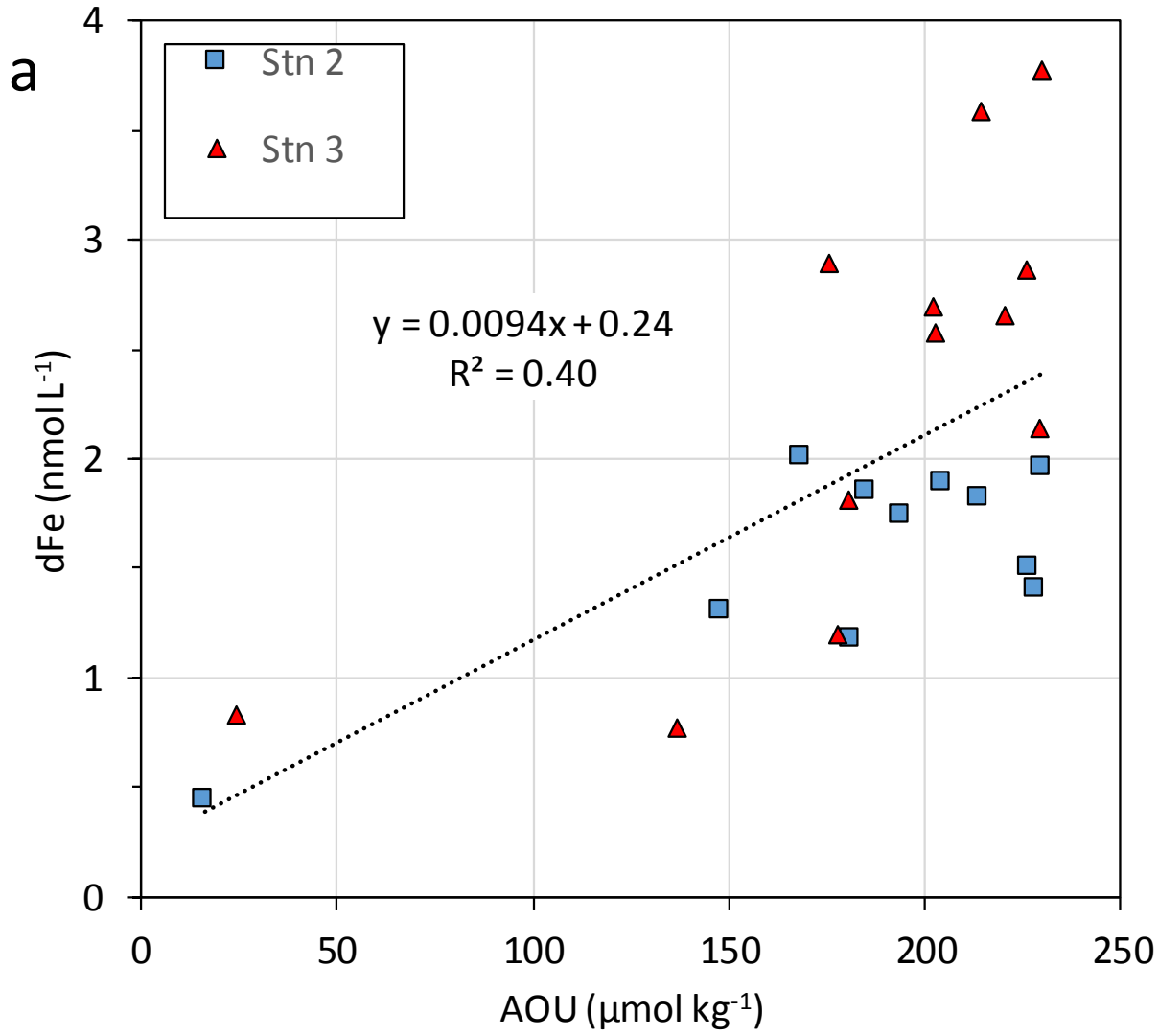
a
Stn 2
Stn 3
y = 0.0094x + 0.24
R² = 0.40
dFe (nmol L-1)
AOU (µmol kg-1)
0
1
2
3
4
0
50
100
150
200
250

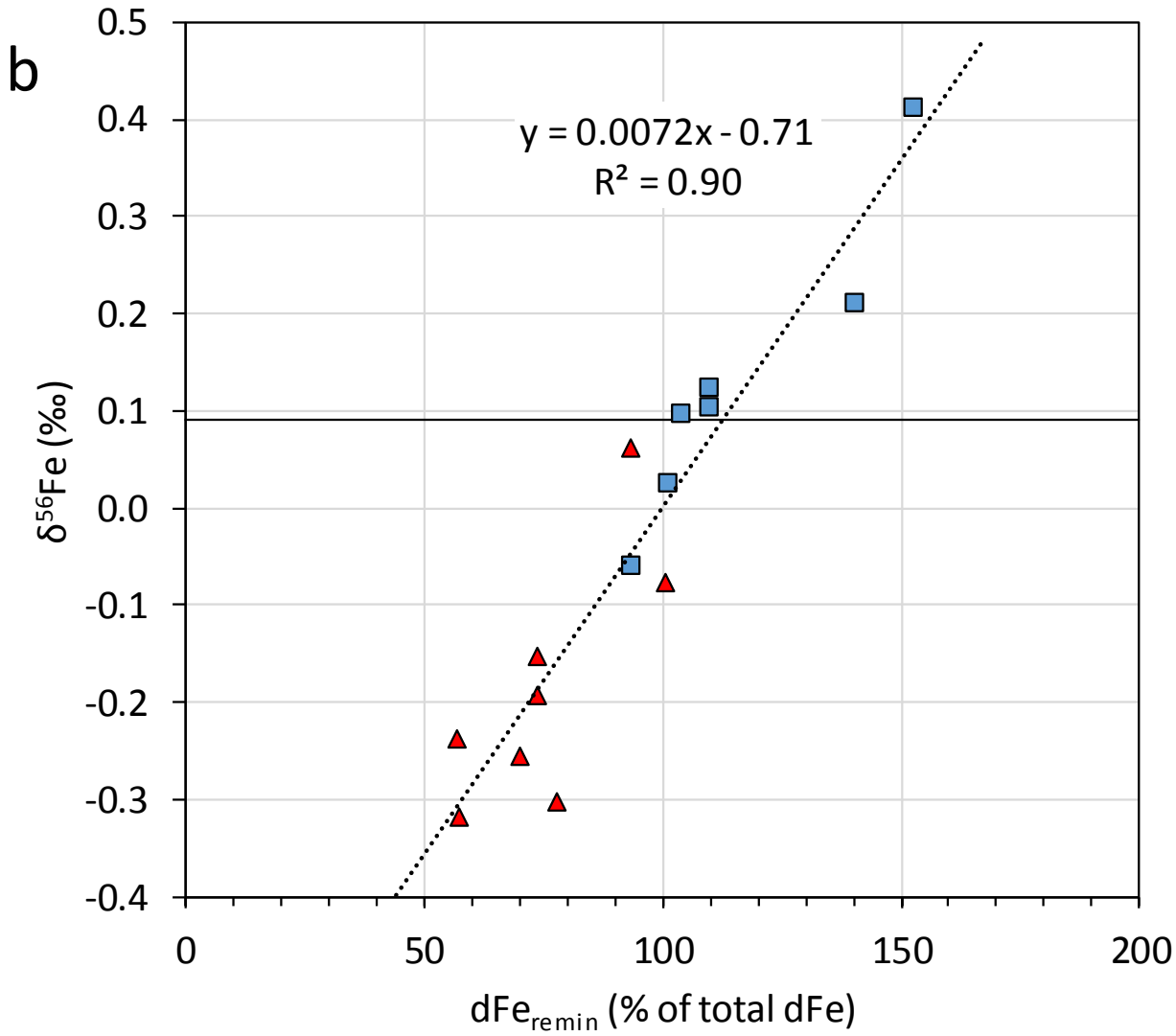
b
y = 0.0072x - 0.71
R² = 0.90
δ56Fe (‰)
dFeremin (% of total dFe)
0.5
0.4
0.3
0.2
0.1
0.0
-0.1
-0.2
-0.3
-0.4
0
50
100
150
200

Figure 7

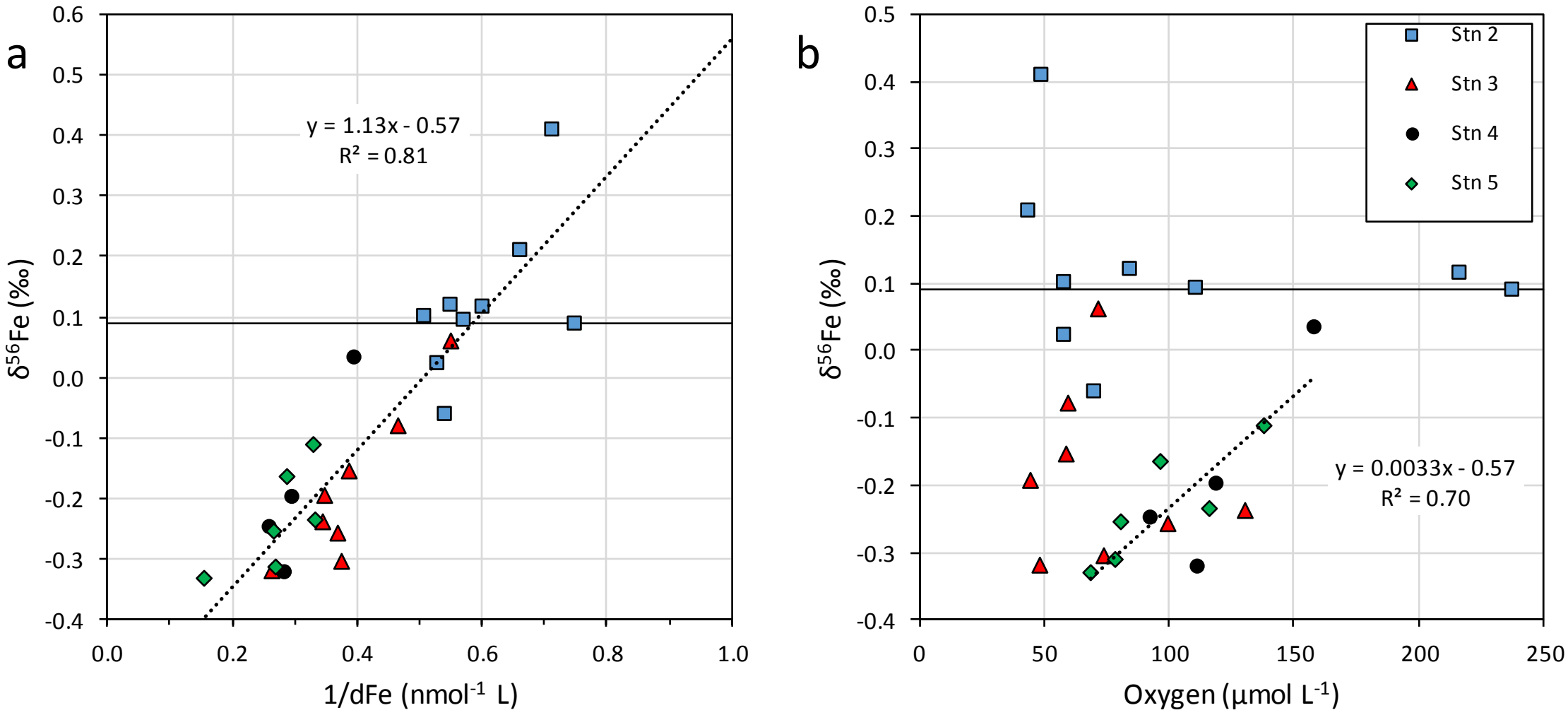
a
y = 1.13x - 0.57
R² = 0.81
δ56Fe (‰)
1/dFe (nmol-1 L)
b
Stn 2
Stn 3
Stn 4
Stn 5
y = 0.0033x - 0.57
R² = 0.70
δ56Fe (‰)
Oxygen (µmol L-1)

Figure 8

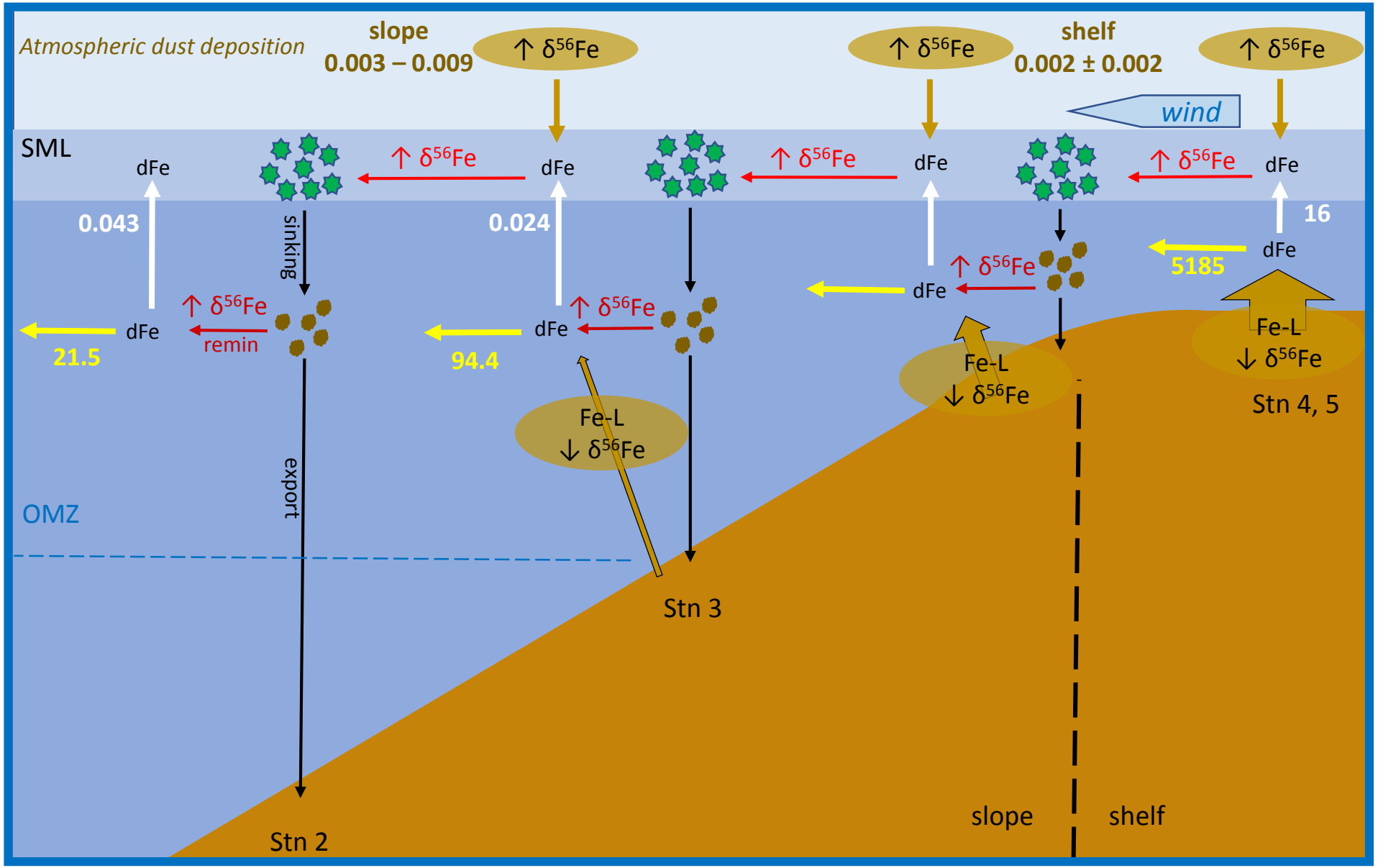
Atmospheric dust deposition
slope
0.003 – 0.009
↑ δ56Fe
↑ δ56Fe
shelf
0.002 ± 0.002
↑ δ56Fe
wind
SML
dFe
↑ δ56Fe
dFe
↑ δ56Fe
dFe
↑ δ56Fe
dFe
0.043
sinking
0.024
16
dFe
5185
↑ δ56Fe
dFe
↑ δ56Fe
remin
dFe
↑ δ56Fe
dFe
21.5
94.4
Fe-L
↓ δ56Fe
Fe-L
↓ δ56Fe
Fe-L
↓ δ56Fe
Stn 4, 5
OMZ
export
Stn 3
Stn 2
slope
shelf